REPORT

Tsunami hazard screening for the Uummannaq fjord system - Greenland

HAZARD SCENARIO SIMULATIONS AND 2017 EVENT HINDCAST

DOC.NO. 20200823-01-R
REV.NO. 0 / 2021-03-26

NORWEGIAN GEOTECHNICAL INSTITUTE
NGI.NO

Project

Project title:	Tsunami hazard screening for the Uummannaq fjord system - Greenland
Document title:	Hazard scenario simulations and 2017 event hindcast
Document no.:	20200823-01-R
Date:	2021-03-26
Revision no. /rev. date:	0 /

Client

Client:	GEUS - De nationale geologiske undersøgelser for Danmark og Grønland
Client contact person:	Jens Jørgen Møller
Contract reference:	Proposal with CTR's 1-2 signed 2/12-2020, signed CTR3

for NGI

Project manager:	Finn Løvholt
Prepared by:	Finn Løvholt
Reviewed by:	Sylfest Glimsdal and Carl Harbitz

Executive Summary

Based on a request from GEUS to carry out a tsunami hazard analysis for the Uummannaq fjord system in western Greenland, NGI has performed numerical simulations of tsunamis that may be triggered by potential collapses of unstable rock slopes. In addition, a modelling hindcast of the 2017 Karrat fjord tsunami is included. The tsunami run-up is quantified at eight locations, Nuugaatsiaq, Illorsuit, Qaarsut, Niaqornat, Uummannaq, Saattut, Ukkusissat, and Ikerasak. In the present study, scenario hazard analysis is based on predefined landslide volumes in agreement with GEUS. Both the probability of failure and the possibility of tsunami generation from other volumes are outside the scope of this study.

A landslide tsunami impacted several coastal communities in Karratfjorden, western Greenland on June 17, 2017, and caused four fatalities in the village of Nuugaatsiaq. A numerical simulation of the 2017 tsunami is presented. The model closely agrees with observations of tsunami run-up heights, observations of tsunami arrival times, and wave periods. The model of the 2017 tsunami was further used to calibrate the tsunami hazard models for the unstable rock slopes.

Location	Run-up height range – Karrat 3, 524 Mm^3 volume – high estimate scenario	Run-up height range – Karrat 3, 412 Mm^3 volume – high estimate scenario	Arrival time – first wave
Nuugaatsiaq	35 – 72 m	30 – 70 m	7 min
Illorsuit	18 – 41 m	17 – 33 m	13 min
Qaarsut	9 – 21 m	7 – 18 m	26 min
Niaqornat	9 – 15 m	7 – 12 m	23 min
Uummannaq	4 – 12 m	4 – 11 m	30 min
Saattut	3 – 8.5 m	2 – 8.5 m	35 min
Ukkusissat	3.5 – 5.5 m	3 – 4.5 m	26 min
Ikerasak	2.5 – 9 m	2 – 8 m	38 min

The modelling herein quantifies large tsunami run-up heights caused by potential landslides originating from the unstable rock slope complex named Karrat 3 located a few kilometres west of the 2017 failure location. The Karrat 3 volume may potentially be more than ten times greater than what was released during the tsunami-genic landslide in 2017, and the resulting tsunami could impact local communities more severely and widely than in 2017. Run-up heights for the scenarios giving the highest estimates for each study location due to Karrat 3 are presented in the table above. The tabulated spatial variability ranges show that the run-up can have a considerable spatial variability within a given location for each landslide scenario. Extreme run-up heights are found for Nuugaatsiaq, Illorsuit, Niaqornat, completely inundating these settlement areas. Very high run-up heights are also found for two other locations at intermediate distances (Qaarsut and Uummannaq), while the inundation is more confined in Saattut, Ukkusissat and Ikerasak. The large modelled run-up heights, involving extreme run-up heights and relatively short arrival times for the nearby locations, demonstrate the need for better understanding of the risk as well as risk-reducing measures.

The two other investigated landslide volumes Karrat 1 and Karrat 2 pose a smaller tsunami hazard towards Nuugaatsiaq (4 m run-up height) and Illorsuit (1.9 m run-up height). Tsunamis originating from these landslides are not expected to cause inundation towards the six other more distant locations.

The figure below shows examples of the maximum horizontal inundation distances due to two different Karrat 3 landslide volumes, for the location closest to the landslide (Nuugaatsiaq) and the most populous location of Uummannaq. The red and yellow lines show the results for the largest and smaller volume respectively. The solid and dashed lines indicate the high and low estimates for each case (based on different combinations of input parameter values) indicating the uncertainty range. Run-up can be higher in the presence of high tides.

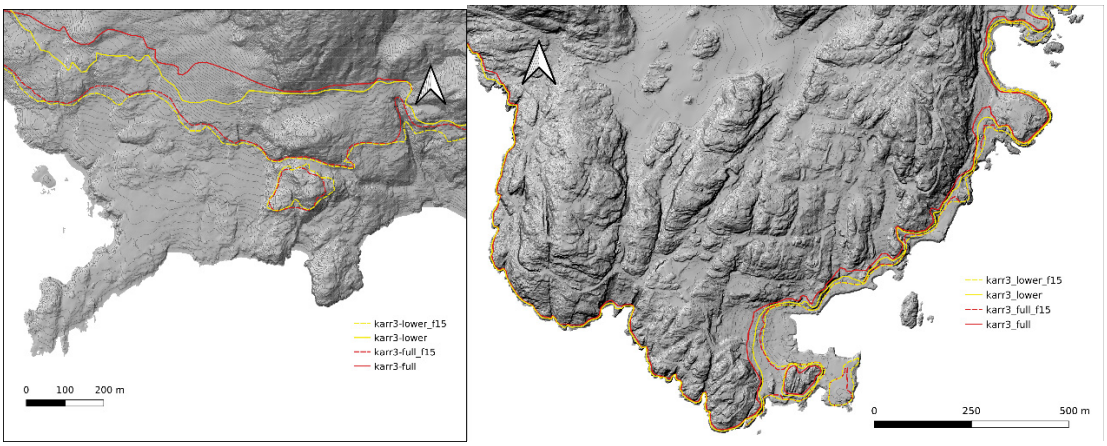

Observations of the 2017 tsunami conclude that, for this particular event, the first wave was not the highest one. Typically, the highest wave appeared several minutes after the first arrival. Therefore, the first wave can potentially provide an opportunity for people to self-evacuate when later wave cycle arrives. Hence, it is important to raise awareness among the local population to commence self-evacuation procedures in case of unusual wave activity. These phenomena may potentially be a pre-cursor of larger waves, even though there is no guarantee that such pre-cursors will take place in the case of a future event.

The main source of uncertainty in this study is related to the landslide dynamics and tsunami generation phase, as well as the likelihood of the large volumes to rapidly fail as a single event. The uncertainty related to the landslide dynamics is partly taken into account here through alternative landslide models. Mapping the 2017 landslide deposit offshore, re-calibration of the 2017 event, and a revised analysis of the given landslide scenarios could potentially reduce uncertainties. Increased geological understanding of the likelihood of failure for different volumetric compartment of the unstable slope would also increase understanding of the hazard.

The second most important source of uncertainty is related to the accuracy of bathymetric grids near the shore. Therefore, obtaining better-quality bathymetric data may also reduce uncertainties for some locations. However, improved bathymetries are not expected to change the overall conclusions of the present study.

Contents

Tables

Figures

Appendix

Review and reference page

1 Introduction

On June 17, 2017, a large landslide tsunami impacted several coastal communities in Karratfjorden, western Greenland, causing severe damage in the nearest village of Nuugaatsiaq, including four fatalities. On slopes adjacent to the 2017 landslide event, several additional unstable volumes have now been discovered. One of these slopes, coined Karrat 3, involves a much larger volume than the event that took place in 2017. The larger landslide volume represents a consequent tsunami threat over a wider region compared to the tsunami in 2017, potentially impacting villages in the Uummannaq fjord system located farther from the rock slope complex than Nuugaatsiaq.

NGI has been contracted by GEUS to investigate the tsunami threat posed by these unstable rock slopes in case of a catastrophic failure. In this report, potential landslide tsunami hazard is quantified at the eight coastal villages Nuugaatsiaq, Illorsuit, Qaarsut, Niaqornat, Uummannaq, Saattut, Ukkusissat, and Ikerasak. For each of these sites, the hazard is quantified through different inundation maps. The probability of occurrence for the different scenarios are not assessed in this report.

An important additional part of the work consists in modelling and understanding the 2017 tsunami event, through comparison of modelling results against empirical run-up observations. In this report, a landslide model is tuned to generate a tsunami that complies with the tsunami run-up observations from 2017. These landslide parameters are subsequently used in the hazard analysis for the unstable rock slope scenarios. Three previously identified unstable rock slopes near the Karrat 2017 landslide were included in this analysis, namely Karrat 1, Karrat 2, and Karrat 3. Karrat 1 and Karrat 2 have volumes of 11 and 13 Mm^3, respectively, both smaller than the 2017 event, while two different volumes (524 and 412 Mm^3) are considered for the Karrat 3 case. Because of the very large potential volume, Karrat 3 carries the largest tsunami threat to distal communities. Hence, Karrat 3 is also given the major emphasis in this report. Modelling uncertainties and implications on the hazard are also discussed through model simulations alternative landslide scenarios, but a rigorous uncertainty treatment and a probabilistic hazard analysis are beyond the scope of this report.

The work is conducted by means of numerical modelling of the landslide dynamics, tsunami generation, propagation, and run-up. This modelling work has been conducted by NGI, in close collaboration with GEUS both with respect to understanding the 2017 event and for designing the hazard scenarios. GEUS has also provided NGI the necessary detailed topo-bathymetric data to carry out the analysis.

The report is organised as follows: Section 2 describes the study area and the main modelling assumptions, and define key technical terms used in this report. Section 3 reviews the 2017 Karrat fjord tsunami and presents results from numerical simulations of the hindcasting of the 2017 event. Section 4 presents the results of the tsunami hazard analysis represented by four different potential landslide volumes, with focus on the run-up heights for the eight different study locations due to a potential catastrophic failure of Karrat 3. Section 5 discusses the results from the hazard analysis as well as potential

sources of uncertainties. In Section 6 we summarise the findings with some brief concluding remarks. Details about models and more detailed modelling results are presented in three appendices, including methods and data (Appendix A), the Karrat 2017 model simulation examples (Appendix B), and scenario simulations (Appendix C).

2 Study area and model set-up

An overview of the Uummannaq fjord system study area is depicted in Figure 2-1, showing also the bathymetric water depth, the approximate area of landslide release, and the eight different locations for inundation modelling, namely:

- Nuugaatsiaq
- Illorsuit
- Qaarsut
- Niaqornat
- Uummannaq
- Saattut
- Ukkusissat
- Ikerasak

The modelling procedure presented in this report combines four modelling steps, from landslide dynamics, tsunami generation, propagation, to inundation. Details of the applied model setup and the combinations of models are given in Appendix A. The tsunami propagation model covers the entire domain shown in Figure 2-1, while the landslide modelling is restricted to a smaller domain close to the landslide release area shown in Figure 2-1. Individual inundation models are applied within each of the black boxes at the eight locations, applying high-resolution datasets to the small innermost rectangle encompassing the settlement area to resolve the detailed inundation pattern to adequate detail (more details about the modelling procedure can be found in Appendix A).

The tsunami analysis is carried out for the 2017 event and for four different potential landslide scenarios that represent potential catastrophic failures of the identified unstable rock slopes. The locations of the different scenarios are shown in Figure 2-2, and the basis for selecting them is briefly discussed below:

- The **Karrat 2017 event**. A volume of 38.5 Mm^3 was used based on the investigation of Svennevig *et al.* (2020). Because the volume involved some uncertainty, supplementary investigations using a larger volume of 48.5 Mm^3 are also included.
- **Karrat 3 full** volume scenario encompassing the entire unstable Karrat 3 rock slope. Based on input from GEUS, a volume of 524 Mm^3 was established.
- **Karrat 3 lower** slope failure scenario that encompasses the lowermost Karrat 3 area where the largest deformations occur based on InSAR measurements. Based on input from GEUS, a volume of 412 Mm^3 was established.

- **Karrat 1** scenario with a volume of 13 Mm^3.
- **Karrat 2** scenario with a volume of 11 Mm^3.

The tsunami generation is linked to the landslide velocity in addition to the landslide volume. This landslide velocity depends on the landslide friction property. Therefore, sensitivity studies with different values of landslide friction angle were carried out to investigate its importance on the tsunami inundation and thus roughly estimate tsunami run-up height uncertainties (see Appendix A for details).

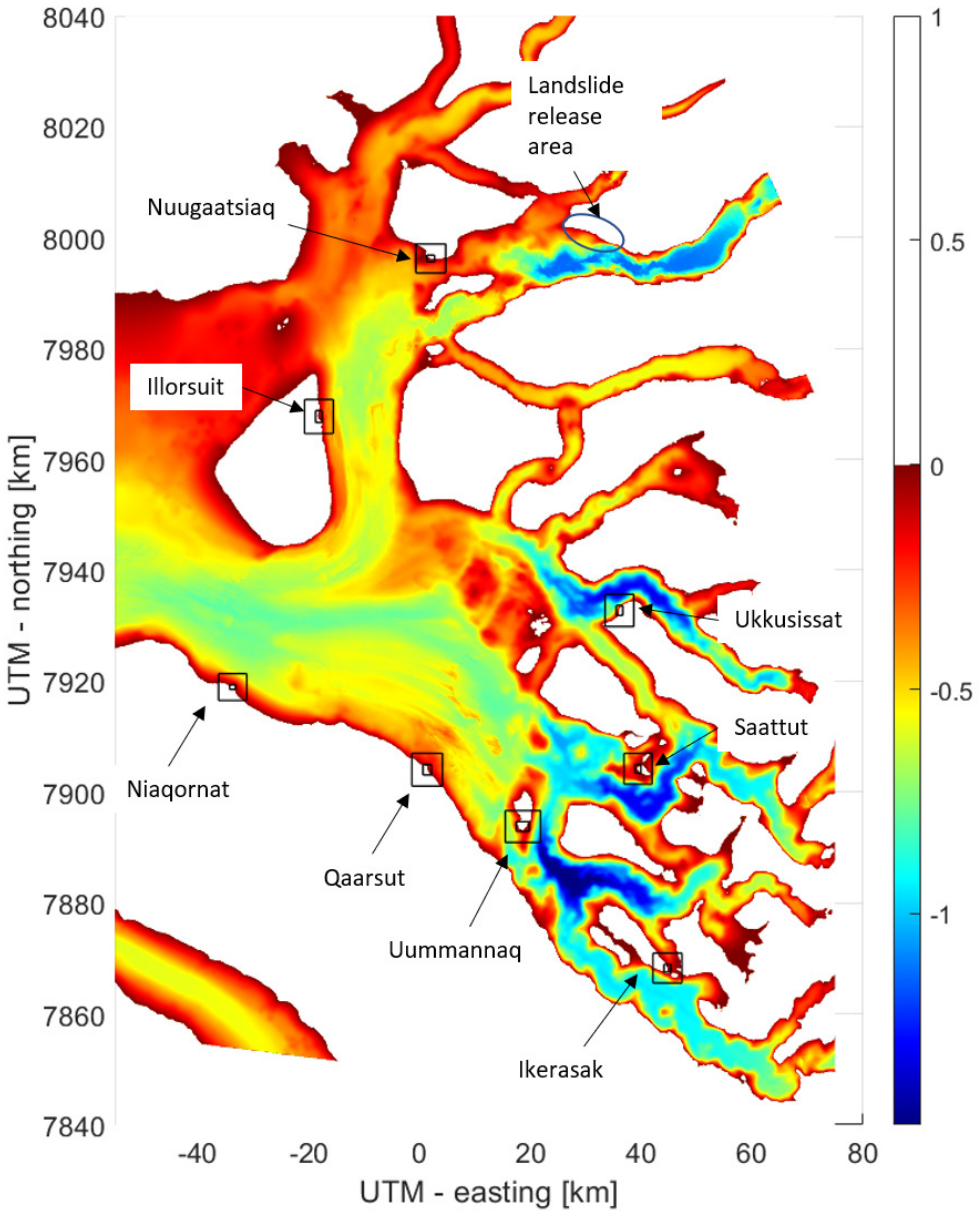

Figure 2-1: Study area, including the location of the unstable rock slope release area including the location of the 2017 landslide (see Figure 2-2) and the locations for high resolution inundation modelling. The colour bar shows the water depth in the fjord in kilometres.

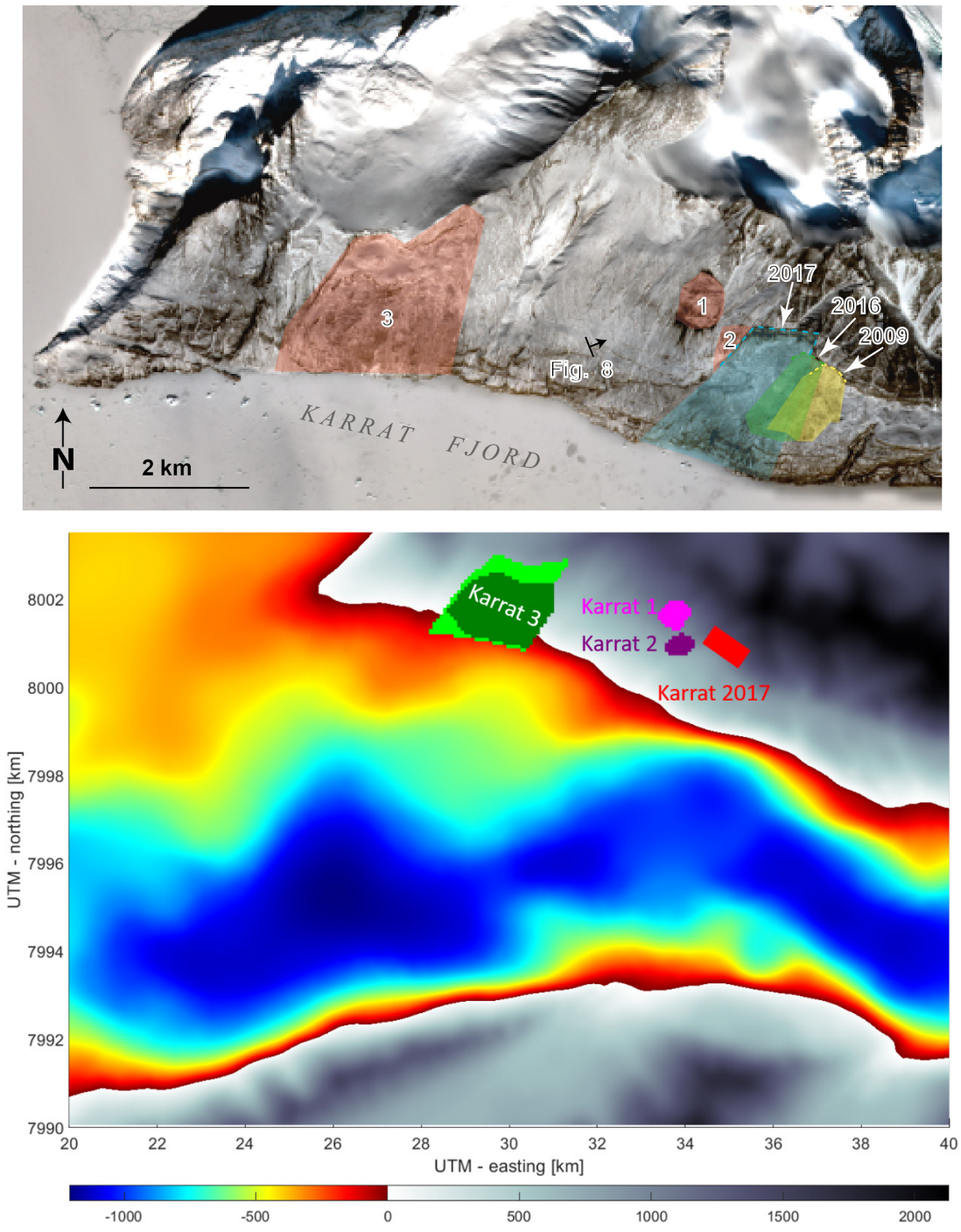

Figure 2-2: The upper panel shows the location of the 2017 event and the identified unstable rock slopes (Svennevig et al., 2020). The lower panel shows the location and extent of the various landslide volumes used for the analysis of the 2017 event (hindcast) and the scenario hazard analysis. For Karrat 3, the light green colour shows the extent of the full volume scenario, while the dark green colour shows the extent of the lower volume scenario.

2.1 Key terms used in this report

- **Maximum inundation height:** The maximum water elevation onshore above mean sea level during the entire tsunami inundation process.
- **Trim line:** Locations of the innermost inundated (wet) point during the tsunami inundation process.
- **Horizontal inundation length:** Horizontal distance from the shoreline to the trim line (measured along the inundation path).
- **Run-up height:** The vertical tsunami height measured above mean sea level at the trim line location.
- **Maximum water elevation:** The maximum water elevation offshore above mean sea level at a given location.
- **Surface elevation:** The vertical elevation of the water surface offshore measured against the mean sea level.
- **Wave height:** Vertical height of the wave offshore measured from trough to crest.
- **Flow depth:** The water height relative to the topographic level.
- **Wave period:** The duration of a full tsunami wave cycle.
- **Landslide run-out distance:** Horizontal travel distance reached by the landslide.
- **Landslide friction angle:** Here, landslide parameter describing the flow resistance in the numerical model; a low friction angle gives a lower resistance to flow and higher landslide velocities.

3 The Karrat 2017 landslide and tsunami

3.1 Event description and reconstruction

The tsunami event occurred on June 17, 2017 at 21.39 local time. Based on a survey of previous scientific investigations of the event (Svennevig *et al.*, 2020; Paris *et al.*, 2019; Strzelecki and Jaskolski, 2020), video footage, and information from GEUS based on eyewitness observations, we obtain the following reconstruction:

Landslide event:

- Recorded by seismic instruments to take place at 21.39 local time on June 17, 2017.
- Estimated to have a volume of 38-40 Mm^3 (Svennevig *et al.*, 2020). A larger slide volume of 50 Mm^3 was used in a modelling attempt of Paris *et al.* (2019) in order to explain the tsunami.

Observations of tsunami heights:

- **Close to landslide area:** Up to 90 m run-up on the opposite coast.
- **Nuugaatsiaq:** The tsunami reached a run-up height of at least 10 m, possibly as high as 12 m at places (Paris *et al.*, 2019; Strzelecki and Jaskolski, 2020; GEUS). The horizontal inundation length is estimated to 150 m. A trim line showing the onshore extent of the wave is presented by Strzelecki and Jaskolski (2020).

- **Illorsuit and Qaarsut**: Tsunami run-up heights of 2-3 m are estimated from interpretations of tsunami videos. The observation in Qaarsut is limited to a highly localized splash close to a single building, and the overall run-up heights are significantly lower.
- **Niaqornat and Uummannaq**: Observations of large "swells".

Observations of tsunami arrival:

- **Nuugaatsiaq:** Reported arrival is 8 minutes after the landslide failure. Information from GEUS through eye witnesses and videos suggests that the highest wave arrived later than the first 2-3 waves. The seismic signal in Nuugaatsiaq provides information of the timing of the wave and wave train (Paris *et al.*, 2019), this could suggest that the maximum wave occurred 10-15 minutes after the first arrival, clearly confirming that the first wave was not the highest one.
- **Illorsuit:** Video recordings (https://www.youtube.com/watch?v=amWshLXe74s) show a wave arrival 25 minutes after the landslide event. Tsunami modelling presented below show that the first wave arrived after 13 minutes, indicating that the first wave may have been small or even unnoticed.
- **Uummannaq:** Large swells were observed 53 minutes after the landslide event. Tsunami modelling presented below show that the wave arrived after 30 minutes, which may again indicate that the first waves may not have been properly noticed. This also hints that it takes even longer delay time for the wave to reach its maximum in far-field locations compared to the sites more proximal to the source such as Nuugaatsiaq and Illorsuit.

Observations of tsunami wave periods:

- **Seismic measurements:** Seismic footprints due to the tsunami from Nuugatsiaq (Paris *et al.*, 2019) reveal a typical wave period of two-three minutes. However, these are measurements of vibrations on the ground, and is thus an integral response from multiple tsunami wave signals across the local fjord and is hence only an indirect measurement.
- **Video recordings:** Video recordings of inundation and drawdown from Nuugaatsiaq (e.g. https://www.youtube.com/watch?v=tWvYFMo2LsQ&t=14s) reveal wave periods of about 1 – 1.5 minutes, a significantly shorter wave period than what the seismic signals suggest.

3.2 Tsunami modelling of the Karrat 2017 event

Using the four-step tsunami modelling procedure described in Appendix A, offshore tsunami wave heights for the entire fjord area and tsunami run-up heights over the whole simulation period for all scenarios were quantified for all the eight study locations. In the cases where the modelling did not cause any significant inundation, also the nearshore maximum water elevation was quantified. This was done for both the 2017 landslide volumes investigated (38.5 Mm^3 and 48.5 Mm^3), and for each scenario landslide volume, using two different values of the landslide friction angle.

For a given study location, the modelled tsunami run-up height varies spatially, and depends also on the landslide parameters. Table 3-1 compares the modelled run-up heights with observations (where available) at the eight study locations. (More details can be found in Appendix B). Figure 3-1 further compares two simulated scenarios against the trimline reported by Strzelecki and Jaskolski (2020) in Nuugaatsiaq for two different landslide simulations. Simulated arrival times for the first wave arrival are given in Table 3-2. We strongly emphasise that for all the study locations, the largest modelled wave arrives significantly (at least 10 minutes) later than the first wave arrival. This is consistent with timing of the maximum wave based on eyewitness observations.

*Table 3-1: Modelled run-up height ranges compared with available observations of run-up height ranges for the two different volumes used for the Karrat 2017 event. *Larger run-up heights ranging from 10-15 m are modelled outside the settlement area. **Observed run-up in southernmost area of the settlement, the higher values in the simulations above 3 m are located north of that. *** Highly localized / splash, lower run-up height in the rest of the adjacent area. ****Simulated maximum water elevation, no significant run-up in simulations.*

Location	Smallest landslide volume (38.5 Mm^3)	Highest landslide volume (48.5 Mm^3)	Observation
Nuugatsiaq*	2.3 – 9.4 m	2.8 – 10.2 m	6 – 10 m
Illorsuit**	1.9 – 4.6 m	2.2 – 5.4 m	2 – 3 m
Qaarsut	0.6 – 1.7 m	1 – 2.1 m	3 m***
Niaqornat	1.2 m	1.5 m	Large swells
Uummannaq	0.5 – 1.4 m	0.6 – 1.8 m	Large swells
Saattut****	0.4 – 0.5 m	0.65 m	-
Ukkusissat	0.8 – 1.0 m	0.8 – 1.2 m	-
Ikerasak****	0.6 – 0.8 m	0.8 – 1.0 m	-

Based on the model simulations, the following comments are provided:

- The modelled run-up heights compare overall well with the reported observations, and with compatible simulated low wave heights at places where there are no wave observations.
- The closest fit with the detailed observations in Nuugaatsiaq is obtained using the greatest landslide volume (48.5 Mm^3). The agreement is best at the east part of the model domain (Figure 3-1), while the western part is underestimated, possibly due to inaccuracies in the bathymetric grid in this area. The greatest landslide volume scenarios also provide closest agreement with the highest wave in Qaarsut, although the observed highly localized (splash) maximum run-up height of 3 m is not matched. In the other parts of Qaarsut, smaller waves can be seen in videos, and these heights overall comply with the model findings also for the smaller volume.
- For Illorsuit, the closest fit is found with the smaller landslide volume (38.5 Mm^3), while the greater volume (48.5 Mm^3) model simulations seems to overestimate the run-up height somewhat.
- For the remaining locations where there are reports of either large swells (no significant inundation) or no wave action, the lower volume seems most compatible.

In particular, limitied run-up heights to 1.8 m in Uummannaq for the largest volume is interpreted as a likely exaggeration compared to wave observations of "large swells".

- Dominant wave periods in the simulations range from 1 to 3 minutes, typically with shorter wave periods in the later part of the wave train. The longest wave period of 3 minutes complies well with the seismic recordings. The highest simulated waves for Nuugaatsiaq have a wave period of about 1.5 minutes, which comply well with the video recordings. The simulated wave periods are hence in close agreement with both types of wave period observations. For some of the distal locations, wave periods can be even longer than 3 minutes.
- The wave arrival times are controlled by the water depth in the fjord system, and the first wave arrival time is therefore estimated almost precisely in the numerical model. The simulated arrival times of the first waves (Table 3-2 give the arrival of the first wave, but in all cases the largest waves appear much later in the simulations). For the three locations where timing of the wave observations is given, the simulations therefore support the eyewitness observations. To this end, the simulations in Nuugaatsiaq suggest that the first "significant wave" (i.e. the first wave that has an amplitude comparable to the maximum wave) appears after 20 minutes. For Illorsuit, the corresponding "first significant wave" appears after approximately 25 minutes. For Uummannaq, this "first significant wave" appears 55 minutes after the landslide was released. However, because of the random character of the later part of the wave train, the maximum wave often appears later than the "first significant wave" in the model simulations. This random wave character implies that the simulations cannot be used to estimate the exact arrival of the maximum wave.

Table 3-2: Simulated first wave arrival times, indicating when the first wave appears in the study area shown in Figure 2-1. Note: The largest wave appears significantly later (at least 10 minutes) than the first one for all locations.

Location	Approximate first wave arrival time - minutes
Nuugaatsiaq	7 min
Illorsuit	13 min
Qaarsut	26 min
Niaqornat	23 min
Uummannaq	30 min
Saattut	35 min
Ukkusissat	26 min
Ikerasak	38 min

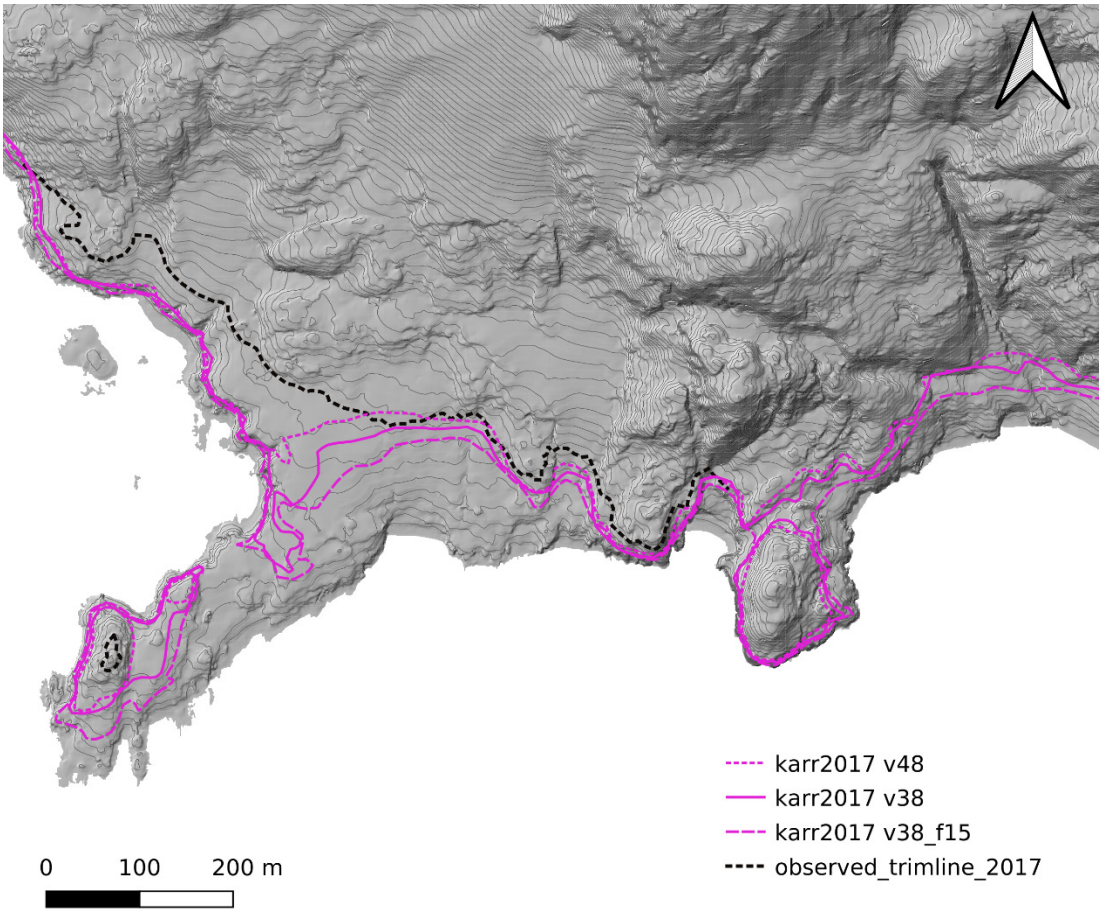

Figure 3-1: Modelled inundation in Nuugaatsiaq and comparison with observed trimline from Strezlecki and Jaskólski (2020). The solid purple line corresponds to the 38.5 Mm³ volume simulations*, the dotted line to the 48.5 Mm³ volume, and the dashed line to 38.5 Mm³ using a landslide friction angle of 15°.*

4 Results from tsunami hazard analysis

Landslide and tsunami propagation simulations were carried out for the four different potential scenario volumes outlined in Section 2. More details of the simulations are given in Appendix C. Examples of the simulated final landslide run-out distance for the two different Karrat 3 landslides causing the waves are given in Figure 4-1. This shows that the landslide may reach the deepest part of the fjord basin, with more than a 10 km run-out distance.

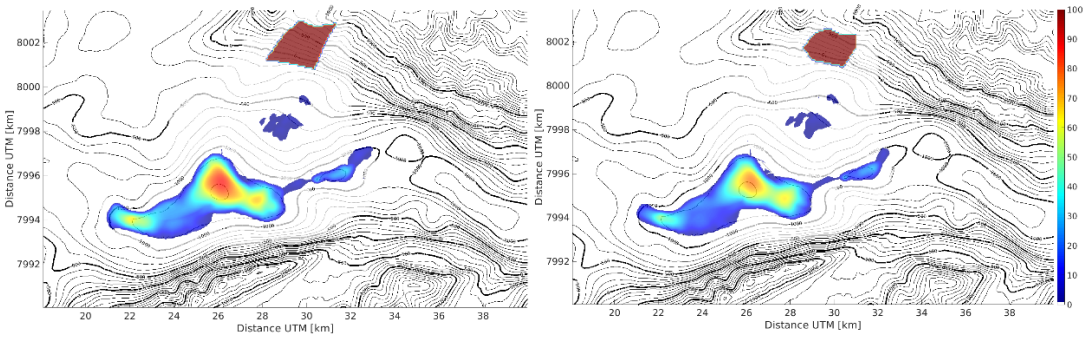

Figure 4-1: Initial landslide thickness (dark red polygons) and examples of simulated final run-out distance for the Karrat 3 scenarios of 524 Mm^3 volume (left) and 412 Mm^3 volume (right). It is noted that the 524 Mm^3 volume has an initial constant thickness of 141 m, while the 412 Mm^3 has an initial constant thickness of 150 m. For the depicted maximum run-out simulations, a friction angle of 5 $^\circ$ is used in the simulations.

To illustrate the wave generation, snapshots of the simulated tsunami surface elevation are shown in Figure 4-2 for four different times, i.e. after 10, 20, 40, and 80 minutes, respectively. The figures apply different colour ranges for the different times to show the wave pattern. However, the maximum wave amplitudes can be considerably larger than indicated by the maximum colour scale. In the landslide area the waves can reach 50-100 m, and off Nuugaatsiaq more than 20 m. This is indicated by the maximum surface elevation caused by the tsunami over the entire duration of the event shown in Figure 4-3.

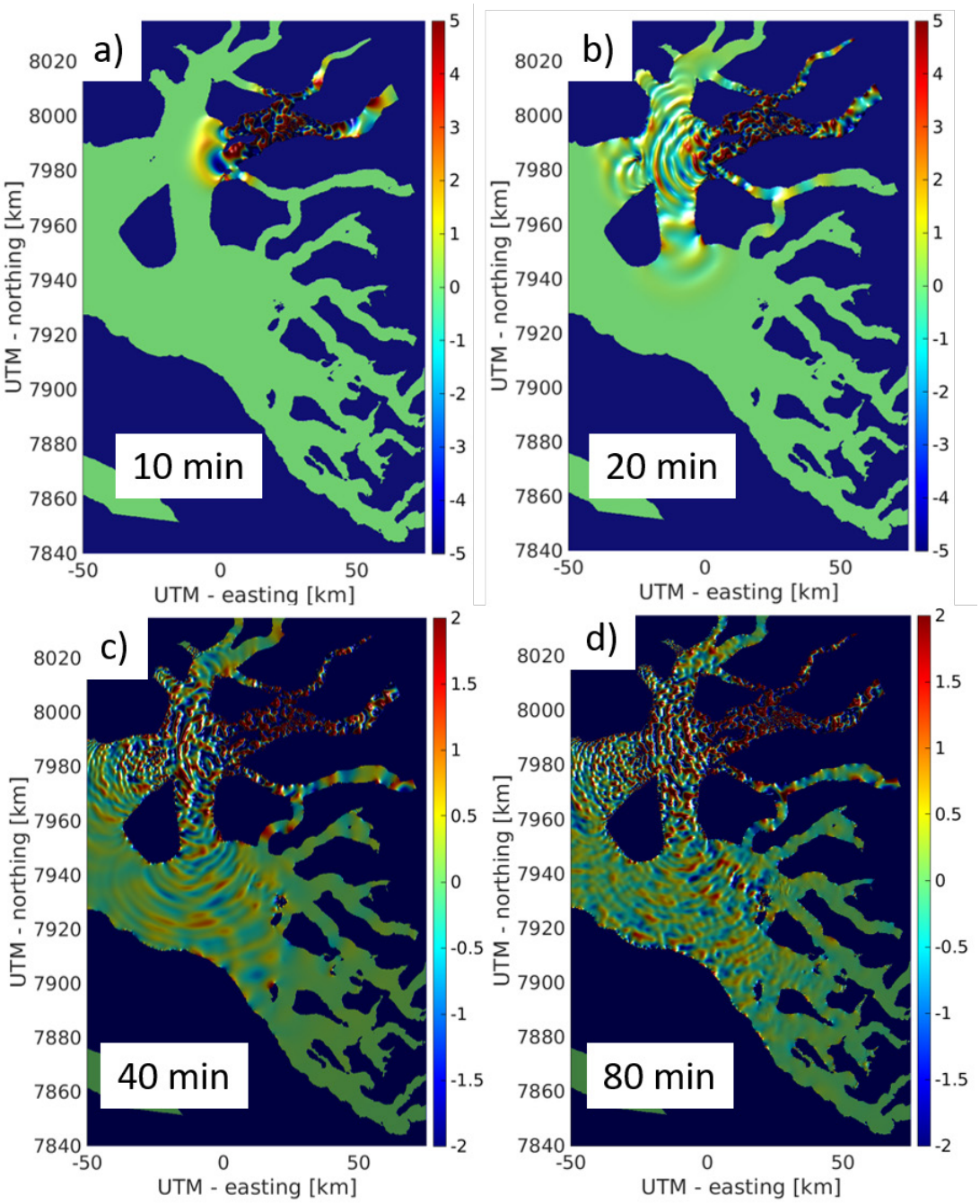

Figure 4-2: Simulated tsunami surface elevation for the 412 Mm^3 scenario using a 10° friction angle after 10, 20, 40, and 80 minutes. Note the differences in colour scale applied to the different surface plots.

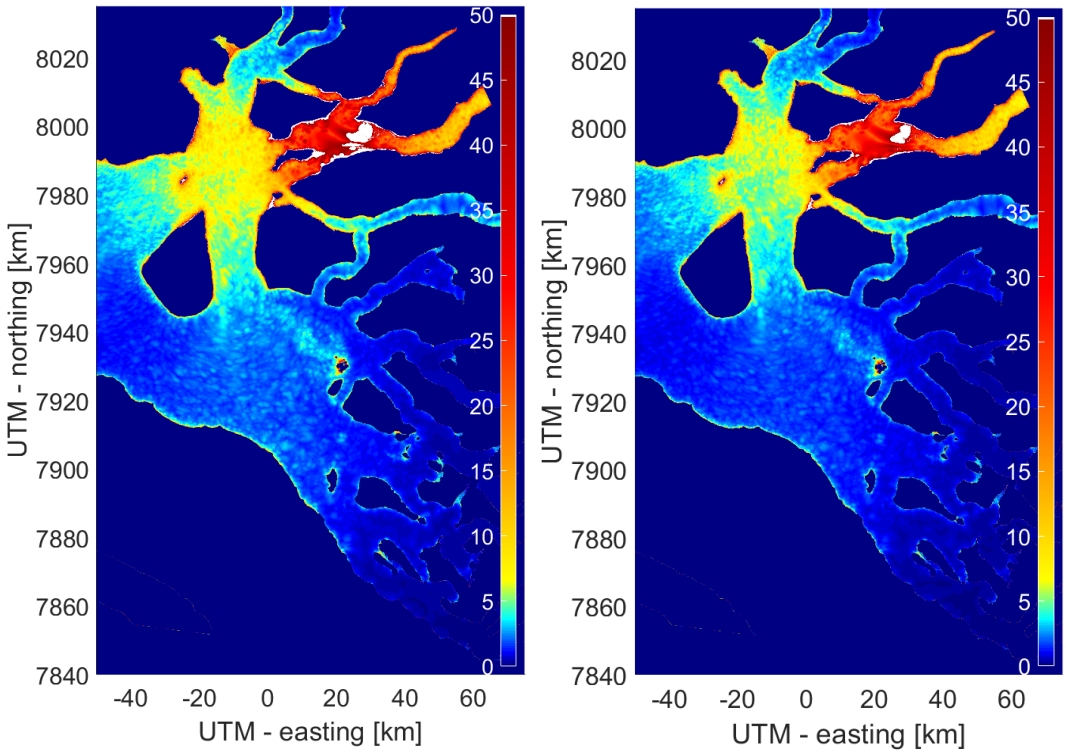

Figure 4-3: Maximum tsunami surface elevations from two Karrat 3 scenarios, high estimate (friction angle 5°). Left 524 Mm³, right 412 Mm³ . We note that the tsunami surface can be higher than the 50 m used as the maximum for the colour bar.

Tsunamis may amplify strongly when they approach the coastline and finally inundate land. To take this effect into account and quantify the inundation, local inundation simulations are carried out for all the study locations. To this end, the simulated range of run-up heights for the two different Karrat 3 volumes are given in Table 4-1 and Table 4-2, while run-up heights for the Karrat 1 and Karrat 2 scenarios are given in Table 4-3. For the Karrat 3 simulations, the tables include both the high and low estimates from the simulations, which highlights the run-up height uncertainty. The high and low estimates are obtained using different landslide parameters (friction angles), see Appendix A and C for details. For the Karrat 1 and Karrat 2 scenarios, several locations have no significant inundation, and for these locations, maximum water elevations are tabulated. The ranges for a given study location refers to the spatial variability within the domain.

*Table 4-1: Local ranges in run-up heights due to the Karrat 3 full scenario (524 Mm^3) for all the study locations, high (5° friction angle) and low (15° friction angle) estimates. All values refer to mean sea level without added tide. The ranges refer to spatial variability within the local domain.*Localized run-up heights in one single bay area, lower values elsewhere.*

Location	High estimate	Low estimate
Nuugaatsiaq	35 – 72 m	19 – 54 m
Illorsuit	18 – 41 m	11 – 25 m
Qaarsut	9 – 21 m	4 – 11 m
Niaqornat	9 – 15 m	4 – 8 m
Uummannaq	4 – 12 m	3 – 8 m
Saattut	3 – 8.5 m*	1.5 – 5 m
Ukkusissat	3.5 – 5.5 m	2.0 – 3.5 m
Ikerasak	2.5 – 9 m*	1.5 – 5 m

*Table 4-2: Local ranges in run-up heights due to the Karrat 3 lower scenario (412 Mm^3) for all the study locations, high (5° friction angle) and low (15° friction angle) estimates. All values refer to mean sea level without added tide. The ranges refer to spatial variability within the local domain. *Localized run-up heights in one single bay area, lower values elsewhere.*

Location	High estimate	Low estimate
Nuugaatsiaq	30 – 70 m	16 – 50 m
Illorsuit	17 – 33 m	12 – 25 m
Qaarsut	7 – 18 m	4 – 10 m
Niaqornat	7 – 12 m	4 – 7.5 m
Uummannaq	4 – 11 m	3 – 7 m
Saattut	2 – 8.5 m*	1.2 – 4.5 m
Ukkusissat	3 – 4.5 m	2.0 – 3.5 m
Ikerasak	2 – 8 m*	1.5 – 4.5 m

*Table 4-3: Maximum water elevations and run-up heights for the Karrat 1 and Karrat 2 scenarios within all study locations. All values refer to mean sea level without added tide. Results are obtained using a friction angle of 5°. *Values refer to maximum water elevations, the modelled wave did not inundate significantly.*

Location	Karrat 1 – 13 Mm^3	Karrat 2 – 11 Mm^3
Nuugaatsiaq	4 m	4 m
Illorsuit	1.7 m	1.9 m
Qaarsut*	0.5 m	0.5 m
Niaqornat*	0.25 m	0.3 m
Uummannaq*	0.6 m	0.6 m
Saattut*	0.15 m	0.17 m
Ukkusissat*	0.2 m	0.15 m
Ikerasak*	0.2 m	0.2 m

Trim lines showing the maximum inland reach of the tsunami for the different locations are shown in Figure 4-4, Figure 4-5, Figure 4-6, and Figure 4-7. As Karrat 1 and Karrat 2 only provided significant inundation in Nuugaatsiaq and Illorsuit, trim lines are only quantified here for these two scenarios. In summary, the maximum horizontal inundation limits in Figure 4-4 through Figure 4-7 include the following information:

i) High estimate (friction angle of 5°) maximum horizontal inundation limit for the full and lower Karrat 3 landslide volume simulations relative to the mean sea level without added tide.
ii) Low estimate (friction angle of 15°) maximum horizontal inundation limit from the full and lower Karrat 3 landslide volume simulations relative to the mean sea level without added tide.
iii) Maximum horizontal inundation limit due to both Karrat 3 landslide volume simulations where a 2 m spring tide is drawn manually on top of the high estimate simulations. Adding this additional tidal elevation was done in agreement with GEUS.
iv) Maximum horizontal inundation limit for Karrat 1 and Karrat 2 landslide volume simulations with a 2 m spring tide drawn manually (only shown for Nuugaatsiaq and Illorsuit in Figure 4-4).

Differences in the horizontal inundation distances between the high estimate (friction angle of 5°) and low estimate (friction angle of 15°; denoted "f15" in the upper panels of the figures) simulations indicate the uncertainty ranges due to the landslide tsunami generation for each site. Additional uncertainty is added by the differences in tidal level. A discussion of the modelling results and related uncertainties is given in Section 5.

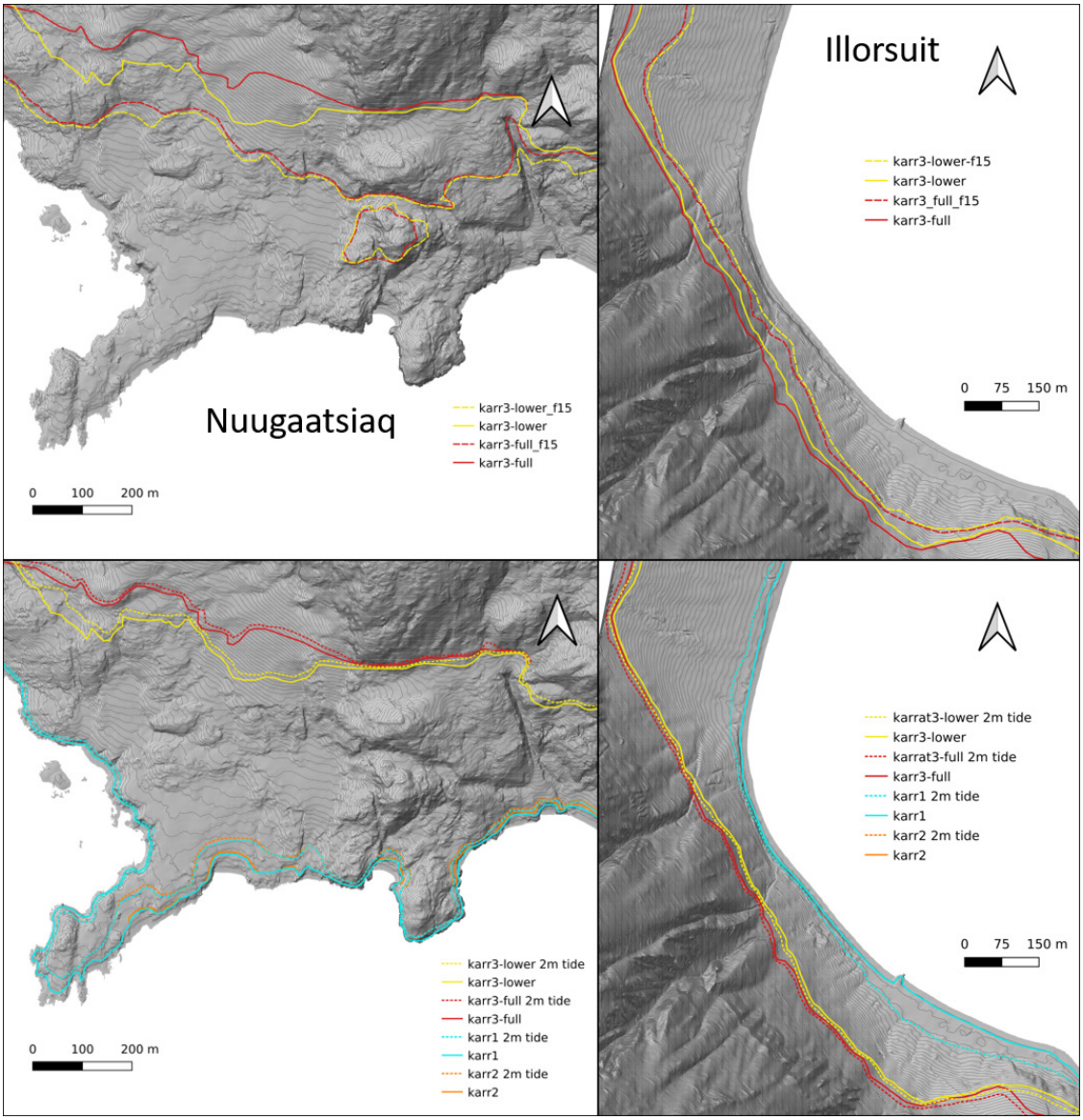

Figure 4-4: Modelled maximum tsunami inundation limits for different scenarios for Nuugaatsiaq (left) and Illorsuit (right). Upper panel, high and low estimates (labelled "f15") for the full and lower Karrat 3 scenarios. Lower panel, high estimates with and without added tide for all scenarios. Red curves refer to Karrat 3 (524 Mm^3), yellow lines to Karrat 3 (412 Mm^3), brown lines to Karrat 2, turquoise lines to Karrat 1.

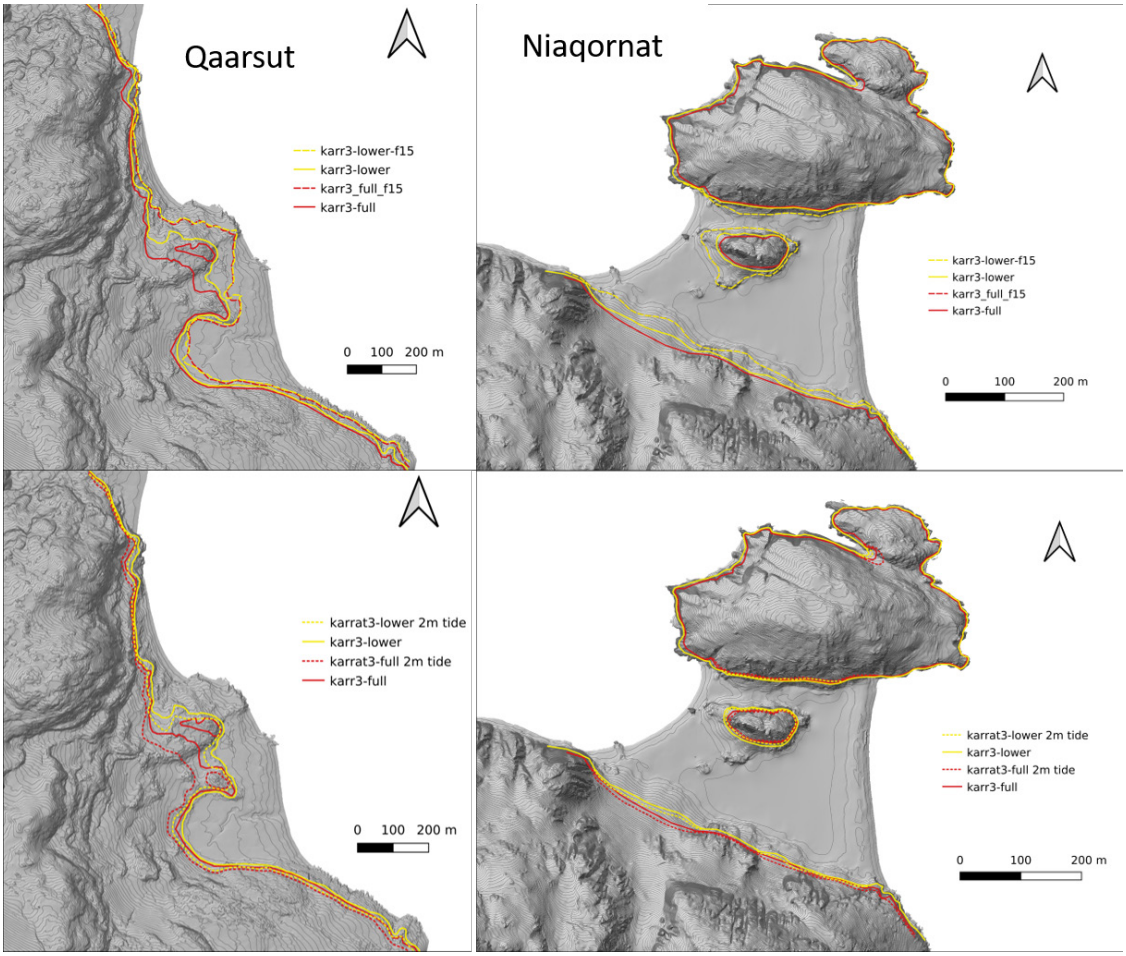

Figure 4-5: Modelled maximum tsunami inundation limits for different scenarios for Qaarsut (left) and Niaqornat (right). Upper panel, high and low (labelled "f15") estimates for the full and lower Karrat 3 volume scenarios. Lower panel, high estimates (friction angle of 5°) with and without added tide for both Karrat 3 volume scenarios. Red lines refer to Karrat 3 (524 Mm^3), yellow lines to Karrat 3 (412 Mm^3).

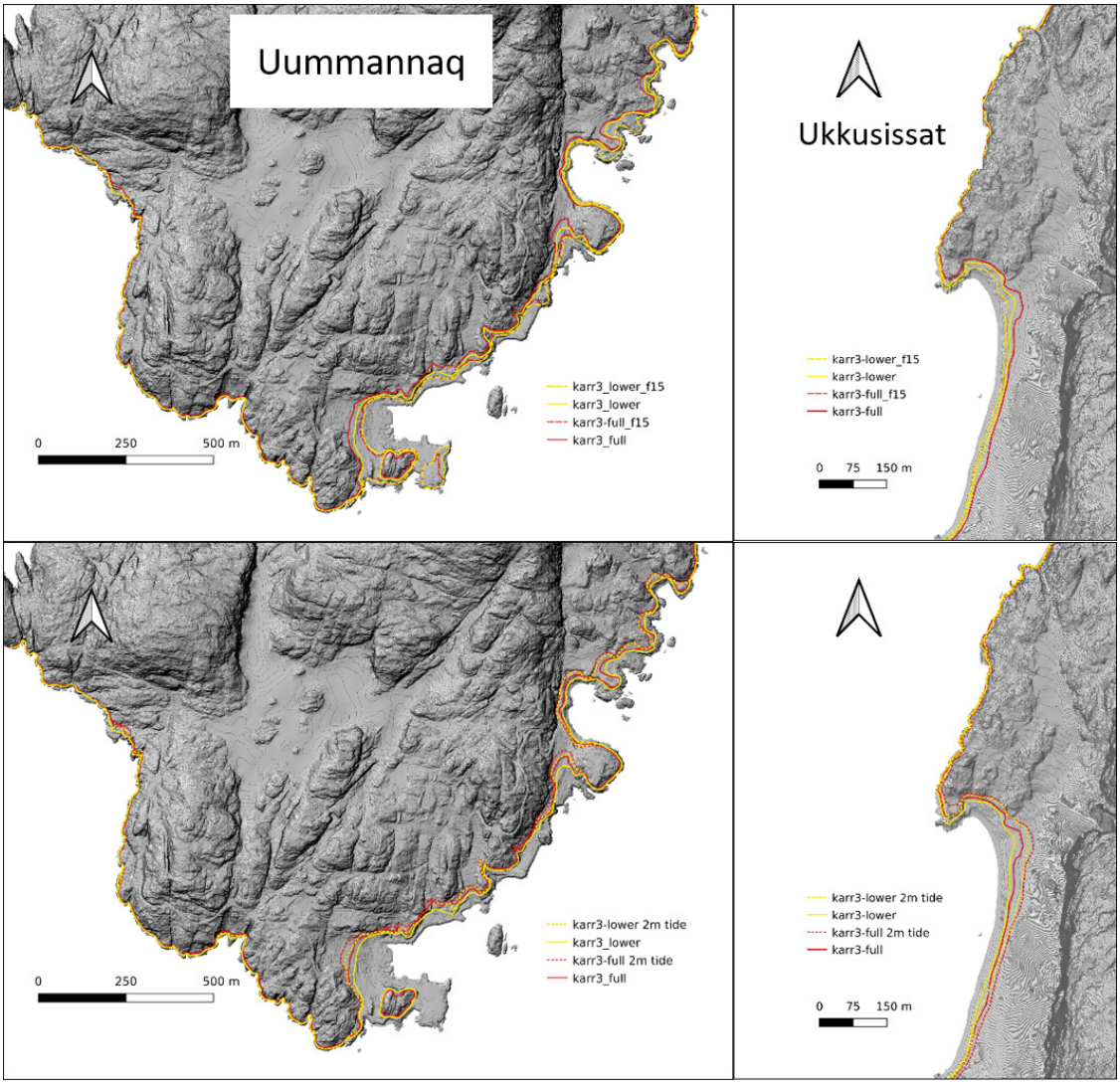

Figure 4-6: Modelled maximum tsunami inundation limits for different scenarios for Uummannaq (left) and Ukkusissat (right). Upper panel, high and low (labelled "f15") estimates for the full and lower Karrat 3 volume scenarios. Lower panel, high estimates (friction angle of 5 °) with and without added tide for both Karrat 3 volume scenarios. Red lines refer to Karrat 3 (524 Mm^3), yellow lines to Karrat 3 (412 Mm^3).

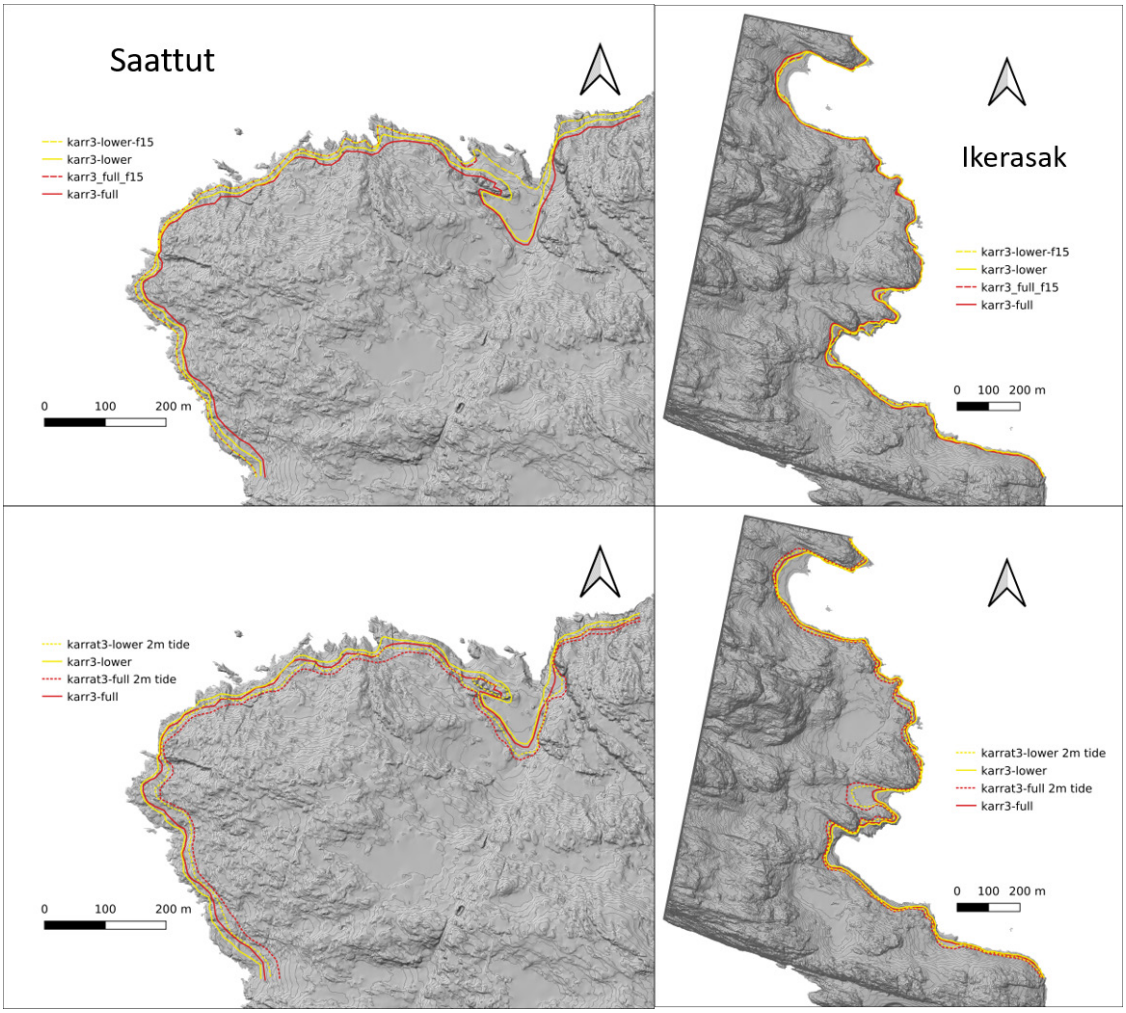

Figure 4-7: Modelled maximum tsunami inundation limits for different scenarios for Saattut (left) and Ikerasak (right). Upper panel, high and low (labelled "f15") estimates for the full and lower Karrat 3 volume scenarios. Lower panel, high estimates (friction angle of 5°) with and without added tide for both Karrat 3 volume scenarios. Red lines refer to Karrat 3 (524 Mm^3), yellow lines to Karrat 3 (412 Mm^3).

5 Discussion of the scenario hazard results

The hazard analysis in Section 4 indicates that a tsunami threat from the unstable Karrat 3 slope is posed to all coastal study sites, with extreme run-up heights for the closest sites. Both investigated Karrat 3 landslide scenario volumes are extremely large, giving for some areas several tens of meters of run-up heights, thus having the potential to generate destructive waves towards many of the villages. In addition, the landslides generate high enough waves in the vicinity of the unstable slopes to represent a danger also towards boats in the open sea a long distance away from the tsunami generation area. The largest landslide volume (524 Mm^3) generates somewhat larger waves than if only the lower slope (412 Mm^3) should fail. There is also an appreciable uncertainty in

the simulations related to the tsunami generation, with significant differences between the high and low estimates in particular for the distal sites.

Comments related to the simulation results for the different study locations for the Karrat 3 scenarios with respect to the tsunami hazard:

- **Nuugaatsiaq and Illorsuit:** In the closest locations of Nuugaatsiaq and Illorsuit, extreme run-up heights are derived, with simulated tsunami run-up heights mostly above 15-20 m, in some areas even exceeding 70 m. Horizontal inundation distances can reach beyond 500 m inland (Nuugaatsiaq). These settlement areas will be completely inundated. The horizontal extent of the inundation in combination with very strong currents implies that structures are not expected to withstand the waves.
- **Qaarsut:** For the more distal Qaarsut village modelling gives extreme run-up heights up to 21 m, with horizontal inundation distances in the southern part of the village up to about 300 m. For the highest estimates a significant part of the settlement area would be inundated, and the large run-up height implies a substantial destructive potential towards buildings and population as for Illorsuit and Nuugaatsiaq. There is a significant uncertainty between the maximum inundation lines derived for the highest estimate and greatest volume, and the low estimate for the smallest volume.
- **Niaqornat:** The simulations for Niaqornat predicts a maximum run-up height of 15 m. Although slightly lower than in Qaarsut, the settlement area is low lying and would be completely inundated with large flow depths providing a high destructive potential.
- **Uummannaq:** Simulations predict high waves for parts of the inhabited area, with run-up as high as 8-12 m and more than a 100 m horizontal inundation in the southernmost bay area where critical infrastructure is located. However, the larger part of Uummannaq is located outside the inundated zone. There is a significant uncertainty in the modelled horizontal inundation.
- **Saattut:** The village of Saattut faces more limited inundation. A maximum run-up height of 7-8.5 m with a horizontal inundation of 100 m is found for the high estimate simulations, but these high waves are confined only to the northern bay area. The shape of the bay seems to amplify the inundation due to focussing. The low estimate simulations give more limited inundation also in the bay area. Along the rest of the coastline, the run-up heights are more limited with typical maximum run-up heights of 2-4 m inundating about 20-40 m inland.
- **Ukkusissat:** Model simulations for Ukkusissat give maximum run-up heights up to 5.5 m, mostly in the bay area. The maximum horizontal inundation limit is about 50-75 m. While the run-up heights and the inundated area are smaller than for all other study sites, the inundation limits encompass several buildings in the village for the high estimate simulations.
- **Ikerasak:** The village of Ikerasak faces run-up heights up to 9 m for the high estimate simulations, but these large heights are restricted to one single bay area, as the high waves are greatly amplified by the local conditions. The run-up height in this bay is much more limited in the low estimate simulations. The remaining area faces moderate waves of 2-4 m height.

Wave arrival: As it was observed for the 2017 tsunami, also the tsunami modelling for the Karrat 3 scenarios indicates that the first wave is not the largest one, and that the largest waves appear several minutes after the first wave, in fact more than 10 minutes later. In all cases, the first wave is a positive elevation, followed by a series of waves cyclically producing drawdowns and inundations. Both modelling and observations of past events in the Karrat fjord indicate a significant likelihood that a Karrat 3 catastrophic failure and subsequent tsunami possibly may follow this pattern. If the first wave is small but still noticeable, it could provide a possibility for people in some areas to self-evacuate. Therefore, awareness building of the population should be stressed towards self-evacuating in cases of unusual wave activity, as the first wave may provide a precursor for subsequent larger waves. However, this point is still indicated with a strong note of caution. First, the waves in particular towards the nearby locations of Nuugaatsiaq and Illorsuit are so damaging that people may not be able to escape anyhow, as the first wave will involve several meters of run-up. Secondly, uncertainties related to the landslide modelling may imply a different behaviour such as more energy content in the first wave. The modelling suggests that only the locations far away from the source have relatively small first wave amplitudes. It should also be noted that self-evacuation based on precursors is not considered a sufficient means and should only complement other risk mitigation measures.

Potential sources of uncertainties and means to reduce them: The main source of uncertainty is related to the landslide dynamics and tsunami generation phase. The model is depth-averaged (see Appendix A) and includes the details of the landslide dynamics and tsunami propagation, while three-dimensional effects such as hydrodynamic cratering are not included. The calibration of the landslide tsunami model to the 2017 tsunami run-up observations clearly reduces this uncertainty. We experience that the modelling process works well for the hazard analysis in several other sites in Norway (Harbitz *et al.*, 2014, Løvholt *et al.*, 2015, Løvholt *et al.*, 2020). On the other hand, the landslide failure is highly complex, and it cannot be ruled out that a future landslide event could evolve differently than the model scenario predictions or even involve features that have not been considered in the models. Mapping of the 2017 landslide deposit offshore, followed by a re-calibration of the 2017 event, and finally revisiting the simulations could potentially reduce model uncertainties. More sophisticated models could also be employed, but running such models are more resource intensive and it is unclear whether they would help reducing uncertainties further.

The second most important source of uncertainty is related to the bathymetric grids near shore. Local bathymetric data were available for Niaqornat, while the quality of the remaining locations was significantly improved by GEUS. The improvement also turned out to have a significant effect on the simulated run-up heights. Obtaining better-quality bathymetric data for the six other locations may reduce uncertainties here, but they are not expected to provide major changes in the overall hazard level. A more rigorous uncertainty treatment can also be examined through *Landslide Probabilistic Tsunami Hazard Analysis* (LPTHA, Løvholt *et al.*, 2020). Increased geological understanding of the likelihood of failure for different volumetric compartments of the unstable slope

would clearly increase our hazard understanding as well, but this is beyond the scope of this project. Finally, we mention that the presence of sea ice is not taken into account in the present analysis. While it is believed to have at least a second order effect on both the tsunami propagation and inundation, it is sparsely studied and difficult to quantify with present models.

Karrat 1 and 2 scenarios: The smaller Karrat 1 and 2 landslides pose smaller threats to Nuugaatsiaq (4 m maximum run-up height) and Illorsuit (1.9 m). They are not likely to generate substantial threats to the six other more distal villages, although they may generate strong currents felt by boats in the shallow parts of the harbours.

6 Concluding remarks

Based on a request from GEUS to carry out a tsunami hazard analysis for the Karrat fjord areas in eastern Greenland, NGI has performed numerical simulations of tsunamis generated by several large landslides identified from unstable rock slopes, as well as a hindcast of the 2017 tsunami event. The tsunami threat has been studied at eight locations, i.e. Nuugaatsiaq, Illorsuit, Qaarsut, Niaqornat, Uummannaq, Saattut, Ukkusissat, and Ikerasak.

The hindcast of the 2017 tsunami reveals good agreement with observed run-up heights from field surveys and videos in the three villages of Nuugaatsiag, Illorsuit, and Qaarsut. The modelling also matches with observations of large waves offshore Niaqornat and Uummannaq and demonstrates sufficiently small waves to be compatible with a lack of wave observations at the most distant locations from the landslide. The simulations further agree with observations of the tsunami arrival times and observed wave periods. The model parameters from the 2017 tsunami simulations were used to calibrate the scenario models.

Three different unstable slope areas named Karrat 1, Karrat 2, and Karrat 3 representing potential landslides able to generate tsunamis, have been studied. The largest tsunami threat is carried by the Karrat 3 volume, of which a potential tsunami represents a significant threat towards all the study locations. The travel times for the tsunami ranges from 7 minutes for the closest location, to 38 minutes for the most distant one, but the largest waves appear much later, more than 10 minutes after the first arrival. Extreme run-up heights above 20-30 m are found for the two nearest locations of Nuugaatsiaq and Illorsuit, while the simulations also reveal more than 10 m run-up heights to the intermediate locations such as Qaarsut, Niaqornat, and Uummannaq, sometimes even up to 20 m. Several locations would be completely inundated. The impact for the three remaining study locations of Saattut, Ukkusissat and Ikerasak shows local maximum run-up heights up to 9 m, but the horizontal inundation is more concentrated than for the other locations.

The Karrat 1 and Karrat 2 volumes pose a smaller tsunami threat towards Nuugaatsiaq (4 m run-up) and Illorsuit (1.9 m run-up). Tsunamis originating from these landslides are not expected to cause inundation in the other locations.

The modelled large run-up heights, involving extreme run-up heights and relatively short arrival times for the nearby locations, demonstrate the need for better understanding of the risk as well as risk-reducing measures. A better understanding of the potential for the full volume failure of the Karrat 3 landslide and assessing the likelihood of less effective wave generation mechanisms such as a cascading slope failure might help to reduce uncertainties and constrain conservativism in the analysis.

In case of the 2017 event, the first wave was not the highest one – the highest wave typically appeared several minutes after the first arrival. In such cases, the first wave (in cases where it is not itself highly destructive) can provide the possibility for people to self-evacuate. Hence, it is important to raise awareness among the local population to commence self-evacuation procedures in case of unusual wave activity, as these phenomena may be a pre-cursor of larger waves, even though there is no guarantee that such precursors will take place in the case of a future event. It should also be noted that self-evacuation based on precursors is not considered a sufficient means and should only complement other risk mitigation measures.

7 References

Harbitz, C.B., Glimsdal, S., Løvholt, F., Kveldsvik, V., Pedersen, G.K., and Jensen, A. (2014). Rockslide tsunamis in complex fjords: from an unstable rock slope at Åkerneset to tsunami risk in western Norway. Coastal engineering, 88, 101-122.

Løvholt, F., Pedersen, G., Harbitz, C.B., Glimsdal, S., and Kim, J. (2015). On the characteristics of landslide tsunamis. Philosophical Transactions of the Royal Society A: Mathematical, Physical and Engineering Sciences, 373(2053), 20140376.

Løvholt, F., Glimsdal, S., and Harbitz, C.B. (2020). On the landslide tsunami uncertainty and hazard. Landslides, 17, 2301-2315.

Paris, A., Okal, E. A., Guérin, C., Heinrich, P., Schindelé, F., and Hébert, H. (2019). Numerical modeling of the June 17, 2017 landslide and tsunami events in Karrat Fjord, West Greenland. Pure and Applied Geophysics, 176(7), 3035-3057.

Svennevig, K., Dahl-Jensen, T., Keiding, M., Merryman Boncori, J.P., Larsen, T.B., Salehi, S., Solgaard, A.M., and Voss, P.H. (2020). Evolution of events before and after the 17 June 2017 rock avalanche at Karrat Fjord, West Greenland–a multidisciplinary approach to detecting and locating unstable rock slopes in a remote Arctic area. Earth Surface Dynamics, 8(4), 1021-1038.

Strzelecki, M.C., and Jaskólski, M.W. (2020). Arctic tsunamis threaten coastal landscapes and communities–survey of Karrat Isfjord 2017 tsunami effects in Nuugaatsiaq, western Greenland. Natural Hazards and Earth System Sciences, 20(9), 2521-2534.

Appendix A

LANDSLIDE AND TSUNAMI MODEL METHODOLOGY

Contents

A1 Modelling set up

The goal of the modelling is to provide inundation maps for different landslide scenarios. The landslide scenarios can have different volumes and material properties, that in turn govern their speed. The tsunamigenic strength of subaerial landslides impacting water typically increases with the landslide volume and speed of the landslide, as well as details related to how the landslide moves. Hence, the tsunami modelling must take into account the rate and extent the landslide motion displaces water. The modelling procedures used in this report follows the descriptions of Løvholt et al. (2010, 2015, 2020), and includes a model for the landslide dynamics (Section A3), a model for conveying the landslide displacement into wave generation (Section A4), a model for the tsunami propagation in the fjord system and open sea (Section A5), and a local tsunami inundation model that takes into account the detailed topography and flow pattern at the study sites (Section A6). The individual models are described in the subsections below. These subsections also describe the modelling set-up, background data, computational grids, etc. In addition, we describe the background datasets for this report in Section A2.

A2 Background, available datasets, and inputs

The following datasets were provided by GEUS and used in the analysis:

- A 100 m resolution bathymetry covering the Uummannaq fjord. This was used to set up the grid for the tsunami propagation model.
- A combined 80 topo-bathymetric map of the Uummannaq fjord. This was used for setting up the grids for the landslide dynamics model and for the coarse grid topo-bathymetric data for inundation simulations.
- Intermediately high-resolution bathymetric data for the study sites. In particular, higher resolution datasets were available for Niaqornat and Uummannaq. For other sites, the 80 m resolution datasets were used as a basis for setting up bathymetric grids for the inundation computations. Improved quality grids for these areas were provided by GEUS for all study sites except for Saattut and Ukkusissat.
- High resolution (0.5 m) topographic data for the eight different study sites, which was used to set up the high-resolution topography grids for the local inundation models.
- Literature (Svennevig et al., 2020; Paris et al., 2019; Strzelecki and Jaskolski 2020), videos and other observations as background for reconstructing the Karrat 2017 landslide and tsunami. This includes landslide volume configurations, measured seismic footprint of the tsunami, timing of the tsunami arrival, run-up heights, trimline etc.

A3 Landslide dynamics model

The landslide model VoellmyClaw (Kim, 2014) is used to model the landslide dynamics. VoellmyClaw is vertically depth averaged, meaning that the landslide thickness is describe numerically with single cell values for each horizontal coordinate. This model is developed for so called granular type landslides that encompass different types of rheologies including subaerial rock slides. The Voellmy model is described by two parameters, the friction angle ϕ, and the quadratic friction coefficient ξ. In this report, we show results with simulations using three different values of ϕ, 5°, 10°, and 15°. These values were established by carrying out several tsunami simulations with different friction angles and comparing the findings with the 2017 event. Additional simulations using higher friction angles (20 and 30°) and lower quadratic friction coefficients was also carried out in the initial phase of the project, but these were not used in the final hazard analysis as they led to too small tsunami heights in hindcasting attempts for the 2017 tsunami.

The landslide dynamics model uses the initial landslide thickness covering the unstable slope area as input. The landslide simulations are carried out on the combined 80 m topo-bathymetric grid provided for Karratfjorden by GEUS. For the landslide simulations, this grid was cut to encompass the local region around the slide and refined to a 20 m grid resolution. The landslide simulations were carried out up to 240 s, and the landslide thickness was exported every 2 s as the input source for generating the tsunami.

A4 Tsunami generation model

When the landslide moves along the sea bottom, it sets up a water displacement that causes the wave. The tsunami generation model used here takes this effect into account, following the description of Løvholt et al. (2015). This model takes into account the hydrodynamic wave surface response due to volumetric seafloor deformations using full potential theory based on Kajiura's model (Kajiura, 1963), but is different from Kajiura as it is time dependent. Typically, the size of landslide disturbance on the bottom is distributed over at least 2-3 water depths, which means that the water column acts as a smoothing filter. This process goes on continuously while the landslide is progressing, at each time step of the simulation, continuously updating the surface elevation in the tsunami propagation model (described in Section A5). It is stressed that this model is linearized, and hence does not take into account the splashing and cratering process during the slide impact.

A5 Tsunami propagation model

The linear dispersive tsunami propagation model GloBouss (Pedersen and Løvholt, 2008) is used for simulating the wave propagation in the open sea. GloBouss is depth averaged, and takes into account wave frequency dispersion, which implies that shorter

waves travels more slowly than the longer leading wave. Dispersion is particularly important for tsunamis with short wavelengths relative to the water depth, such as those typically induced by subaerial landslides. The short wave-periods reported for the 2017 tsunami and the late arrival of the maximum waves are both likely partly due to frequency dispersion. The wave generation model described in Section A4 is used as a time dependent source model in GloBouss. In turn model outputs from the tsunami propagation model is used as time dependent input models for the tsunami inundation model as described in Section A6.

A6 Tsunami inundation model

The tsunami inundation model ComMIT (Titov et al., 2011) is employed here for simulating tsunami inundation. The ComMIT program uses the depth averaged non-linear shallow water model MOST (Titov and Gonzalez, 1997) as the computational engine for modelling the local tsunami inundation. MOST simulates the tsunami inundation using high resolution grids in two dimensions. For computational feasibility, a set of so-called telescopic grids with increasingly higher grid resolution and smaller domains are used. The grid with the largest extent has coarser resolution than the next inner grid and so on. In the applications employed here, three levels of grids are applied, and grid levels from coarsest to finest are denoted A, B, and C. The inundation is calculated on the C-grid only, and the hazard analysis is therefore based on the model outputs within this grid. The horizontal resolution of the C-grids used here is 5 m. The ComMIT application includes a dynamic coupling between the offshore tsunami propagation model GloBouss and in the inundation model (Løvholt et al., 2010). In this way, the results from the offshore wave propagation is seamlessly connected to the inundation simulations. The offshore wave propagation then acts as a time dependent forcing of the MOST simulation as a function of time along the periphery of the A-grid. Extents of the A and C grids used in this report are shown in the outline of the study are in the main body of this report.

A7 References

Kajiura, K. (1963). The leading wave of a tsunami. Bulletin of the Earthquake Research Institute, University of Tokyo, 41(3), 535-571.

Kim, J. (2014). Finite volume methods for Tsunamis genereated by submarine landslides (Doctoral dissertation, Univ Washington).

Løvholt, F., Pedersen, G., and Glimsdal, S. (2010). Coupling of Dispersive Tsunami Propagation and Shallow Water Coastal Response. The Open Oceanography Journal, 4(1).

Løvholt, F., Pedersen, G., Harbitz, C.B., Glimsdal, S., and Kim, J. (2015). On the characteristics of landslide tsunamis. Philosophical Transactions of the Royal Society A: Mathematical, Physical and Engineering Sciences, 373(2053), 20140376.

Løvholt, F., Glimsdal, S., and Harbitz, C.B. (2020). On the landslide tsunami uncertainty and hazard. Landslides, 17, 2301-2315.

Paris, A., Okal, E.A., Guérin, C., Heinrich, P., Schindelé, F., and Hébert, H. (2019). Numerical modeling of the June 17, 2017 landslide and tsunami events in Karrat Fjord, West Greenland. Pure and Applied Geophysics, 176(7), 3035-3057.

Pedersen, G., and Løvholt, F. (2008). Documentation of a global Boussinesq solver. Preprint series. Mechanics and Applied Mathematics http://urn. nb. no/URN: NBN: no-23418.

Strzelecki, M.C., and Jaskólski, M.W. (2020). Arctic tsunamis threaten coastal landscapes and communities–survey of Karrat Isfjord 2017 tsunami effects in Nuugaatsiaq, western Greenland. Natural Hazards and Earth System Sciences, 20(9), 2521-2534.

Svennevig, K., Dahl-Jensen, T., Keiding, M., Merryman Boncori, J.P., Larsen, T.B., Salehi, S., Solgaard, A.M., and Voss, P.H. (2020). Evolution of events before and after the 17 June 2017 rock avalanche at Karrat Fjord, West Greenland–a multidisciplinary approach to detecting and locating unstable rock slopes in a remote Arctic area. Earth Surface Dynamics, 8(4), 1021-1038.

Titov, V.V., Moore, C.W., Greenslade, D.J.M., Pattiaratchi, C., Badal, R., Synolakis, C. E., and Kânoğlu, U.T.K.U. (2011). A new tool for inundation modeling: Community Modeling Interface for Tsunamis (ComMIT). Pure and Applied Geophysics, 168(11), 2121-2131.

Titov, V.V., and Gonzalez, F.I. (1997). Implementation and testing of the method of splitting tsunami (MOST) model. NOAA technical report.

Appendix B

KARRAT 2017 EVENT SIMULATIONS

Contents

B1 Overview of modelling and assumptions

The landslide, tsunami generation, tsunami propagation, and inundation simulations were carried out using the four-step methodology outlined in Appendix A. Because there was initially some uncertainty related to the landslide volume, two different volumes were used, namely 38.5 Mm^3 (Svennevig et al., 2019) and 48.5 Mm^3 (Paris *et al.*, 2019). The smallest volume is based on a detailed field survey and is believed to the be the best estimate, while the second one is taken from a numerical modelling study (Paris *et al.*, 2019) focussing only on matching the wave amplitudes and frequency of the observed seismic footprint of the wave (see description in the main body of this report). These volumes were placed in the location of the slope failure of the 2017 event as initial conditions for the landslide model. The shapes of the volumes were given an asymmetric Gaussian shape, where the maximum thicknesses were tuned to provide the desired volume. The initial landslide shapes are shown in Figure B1-1.

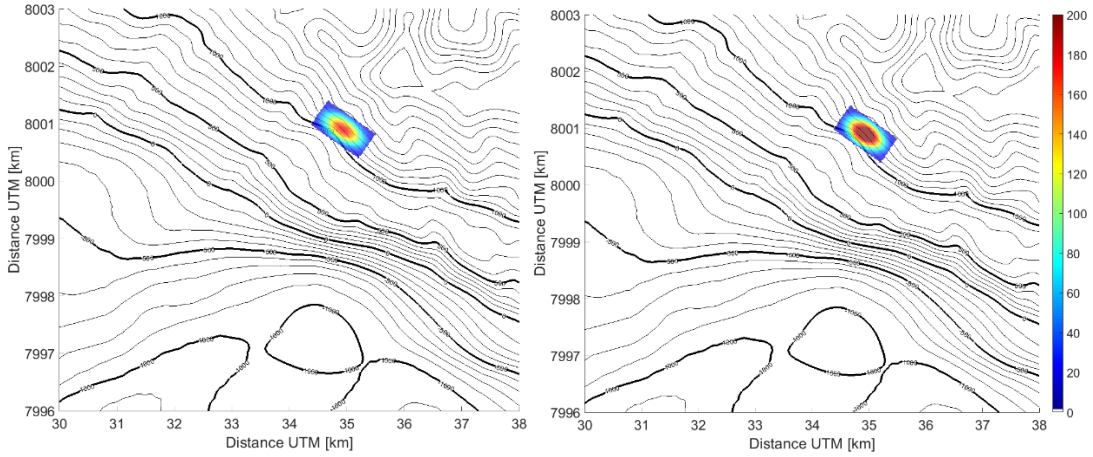

Figure B1-1: Initial slide thicknesses for the Karrat 2017 hindcasts. Left panel, 38.5 Mm^3 for the scenarios, right panel 48.5 Mm^3 scenarios.

Landslide simulations were performed for model friction angles of 5°, 10°, and 15° (the latter was restricted to the 38.5 Mm^3 landslide volume and the subsequent inundation simulations for the three locations with run-up observations), using a grid resolution of 20 m for a run-out duration of 160 s, providing landslide thickness as input to the tsunami simulations every 2 s. The tsunami simulations were carried out on a horizontal grid resolution of 100 m for a total duration of 2 hours. Grid refinement tests were undertaken to check model convergence.

The local inundation simulations where run for a period of 1 hour after the first wave arrival, except for the two distal locations of Ukkusissat and Ikerasak, where the wave build-up took longer time, and the inundation simulations were carried out up to 1.5 hours after the first wave had arrived. The inundation modelling used a Manning friction parameter of $n = 0.03$, and dry land treshold and minium depth values of 0.1 m. Some of the topo-bathymetric data (Uummannaq, Saattut, and Ukkusissat) were

smoothed by a maximum gradient filter in ComMIT to mitigate model induced numerical noise and instabilities.

B2 Comparison with observed heights

A review of the observations of the 2017 tsunami is given in the main text of this report. Below, some more modelling details are given for each individual model simulation run. The main range of maximum run-up heights for each domain for all the simulations conducted is listed in Table B2-1. In addition, trim lines for the maximum values from the 38.5 Mm^3 and 48.5 Mm^3 landslide induced tsunami inundation simulations for the three locations with observations of run-up heights are shown in Figure B2-1 (in the same figure we have also shown a lower bound of the 38.5 Mm^3 scenario with a friction angle of 15° labelled "f15", see also below). The results are in overall good agreement with observations. The 48.5 Mm^3 simulations fits the observations better for Nuugaatsiaq while the 38.5 Mm^3 simulation fits better for Illorsuit, and the 38.5 Mm^3 volume runs also seems more compatible with observations of large swells and no inundation at the other more distal sites. For Nuugaatsiaq the agreement is best at the east part of the model domain, while the western part is underestimated, possibly due to inaccuracies in the bathymetric grid in this area. The location of Qaarsut is matched well, and video observations show moderate run-up heights, with an exception of a highly localized 3 m high run-up, which is not captured in any of the model simulations, although the 48.5 Mm^3 simulations are closest.

There is some sensitivity to the inundation due to the landslide friction angle in the simulations. The 5° and 10° friction angle simulations generally give the best agreement best agreement, as the 15° simulations underestimate the run-up observations in Nuugaatisaq. Hence, the emphasis was put on the simulations using the lowest friction angles.

*Table B2-1: Modelled run-up heights compared with available observations of tsunami heights. *Larger run-up heights ranging from 10-15 m are modelled outside the settlement area. **Observed run-up in southernmost area of the settlement, the higher values in the simulations above 3 m are located north of that. *** Highly localized / splash, lower run-up in the adjacent area. ****Maximum water elevations, no significant run-up.*

Location	**5° friction 38.5 Mm³**	**5° friction 48.5 Mm³**	**10° friction 38.5 Mm³**	**10° friction 48.5 Mm³**	**15° friction 38.5 Mm³**	**Observed run-up**
Nuugaatsiaq*	2.3 – 9.4 m	2.8 – 10.2 m	2.5 – 8.6 m	2.8 – 9.6 m	2 – 8 m	6-10 m
Illorsuit**	1.9 - 4.6 m	2.2 – 5.4 m	1.9 – 4.2 m	2.2 – 4.6 m	1.5 - 3.5 m	2 - 3 m
Qaarsut	0.7 – 1.7 m	1 – 2.1 m	0.6 – 1.5 m	1 – 2.1 m	0.6 - 1.7 m	3 m***
Niaqornat	1.2 m	1.5 m	1 m	1.5 m		Large swells
Uummannaq	0.5 – 1.4 m	0.8 – 1.8 m	0.6 – 1.2 m	0.6 – 1.8 m		Large swells
Saattut****	0.4 m	0.6 m	0.5 m	0.65 m		-
Ukkusissat	0.8 m	0.8 m	1.0 m	1.2 m		-
Ikerasak****	0.8 m	1.0 m	0.6 m	0.8 m		-

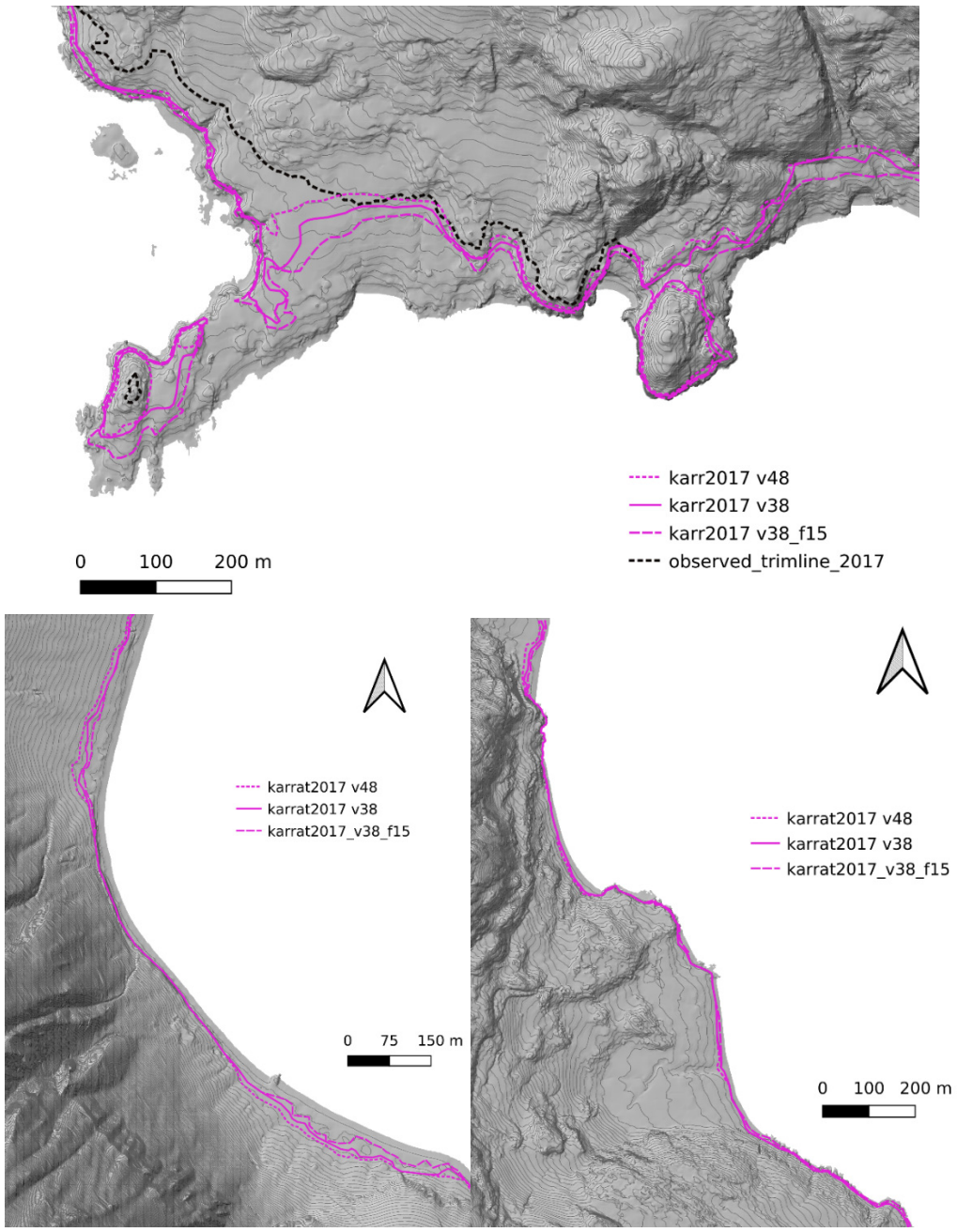

Figure B2-1: Maximum inundation limits (trim lines) for all Karrat 2017 model runs for the locations Nuugaatsiaq (upper panel), Illorsuit (lower left panel), and Qaarsut (lower right panel). The solid lines show trim lines for the largest runup for the volume of 38.5 Mm^3 (lowest of all friction angles), the short-dashed lines are the largest runup for the volume of 48.5 Mm^3 (lowest friction angle 5°) while the long-dashed lines are a lower bound of the simulations (volume 38.5 Mm^3 and friction angle 15°). In the upper panel we have plotted the observed trim line with a black dotted line.

B3 Modelled landslide run-out

Initial and final run-out distances from the VoellmyClaw landslide simulations are shown in Figure B3-1 and Figure B3-2. For the 10° and 15° friction angles the majority of the modelled slide volume is transported to the closest deep basin below the slide area, with a smaller part of the landslide for 10° spilling over to the adjacent basin. For this scenario, a minor part of the slide volume ran out of the computational domain, but this do not influence the wave generation significantly as the major part of the wave generation takes place in the first part of the slide motion after the landslide has entered water. For the 5° friction angle simulations, a larger part of the slide volume has spilled over to the adjacent basin, and the landslide has not come entirely to rest after the 160 s of slide motion simulations. However, the main generation has already taken place at this stage.

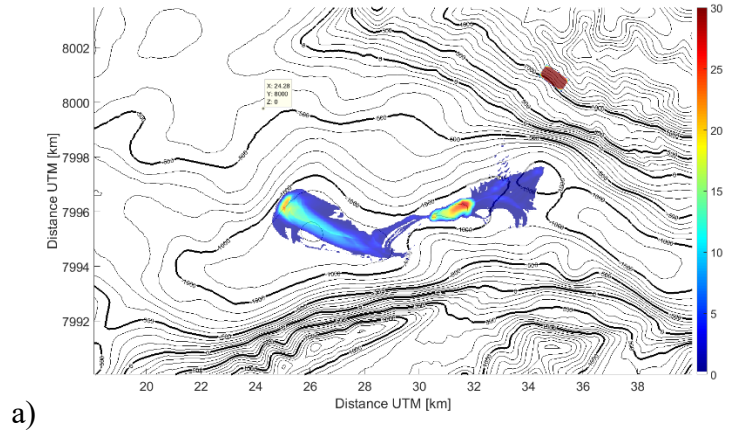

a)

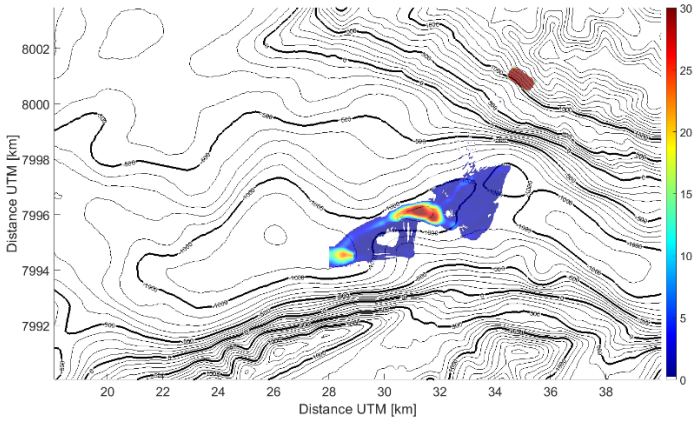

b)

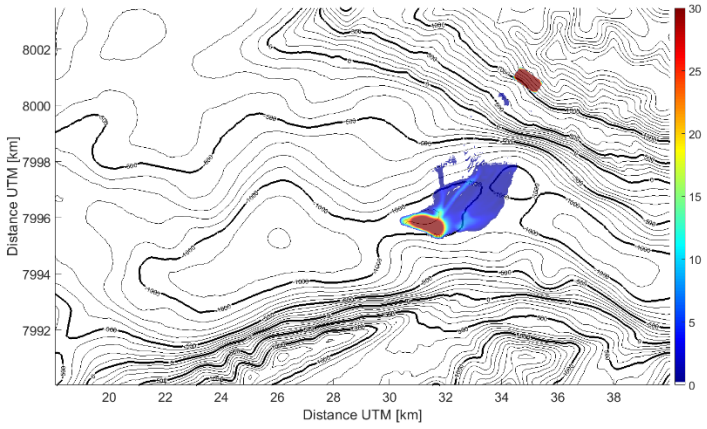

c)

Figure B3-1: Final landslide run-out distance for the 38.5 Mm³ volume simulations using the three different friction angles, a) 5°, b) 10°, and c) 15°.

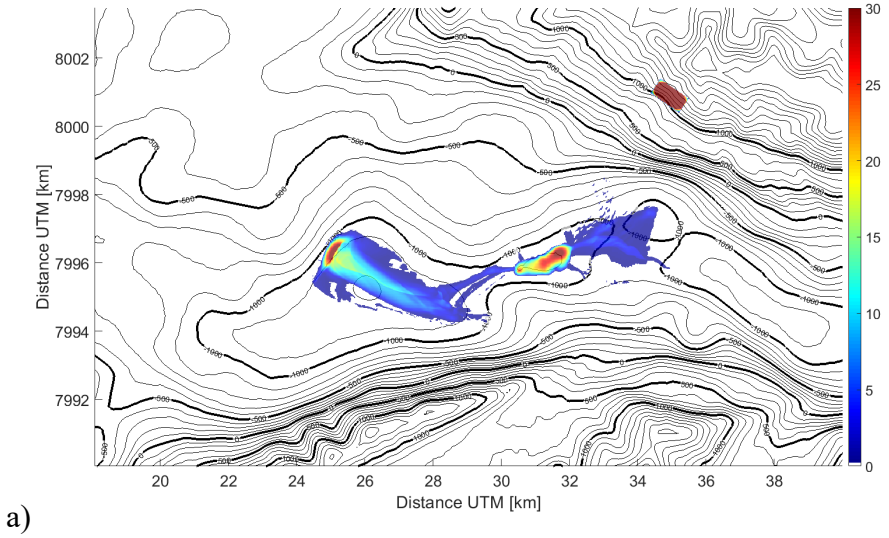

a)

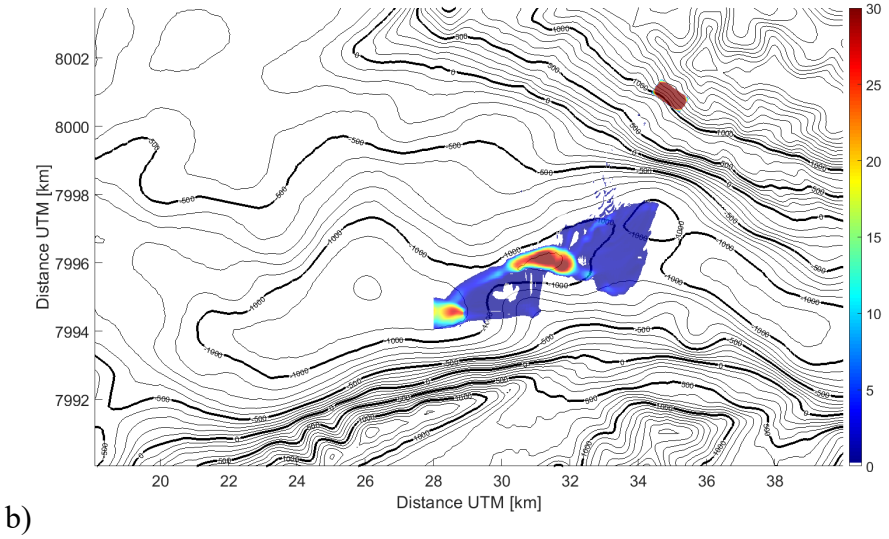

b)

Figure B3-2: Final landslide run-out distance for the 48.5 Mm³ volume simulations using the two different friction angles for a) 5 ° and b) 10 °.

B4 Scenario maximum inundation heights

Below, examples of tsunami maximum inundation maps for each of the study locations are shown for one of the simulations, the 38.5 Mm^3 volume using a 10° friction angle. The figures show the maximum inundation heights (onshore values) and maximum water elevations (offshore values) over the entire simulation period with different colour ranges measured towards the shoreline. As shown, the inundation height can vary substantially within a given location depending on the local topography and bathymetry. Figure B4-1 shows inundation heights for Nuugaatsiaq and Illorsuit, Figure B4-2 for Qaarsut and Niaqornat, Figure B4-3 for Uummannaq and Ukkusissat, and Figure B4-4 for Saattut and Ikerasak.

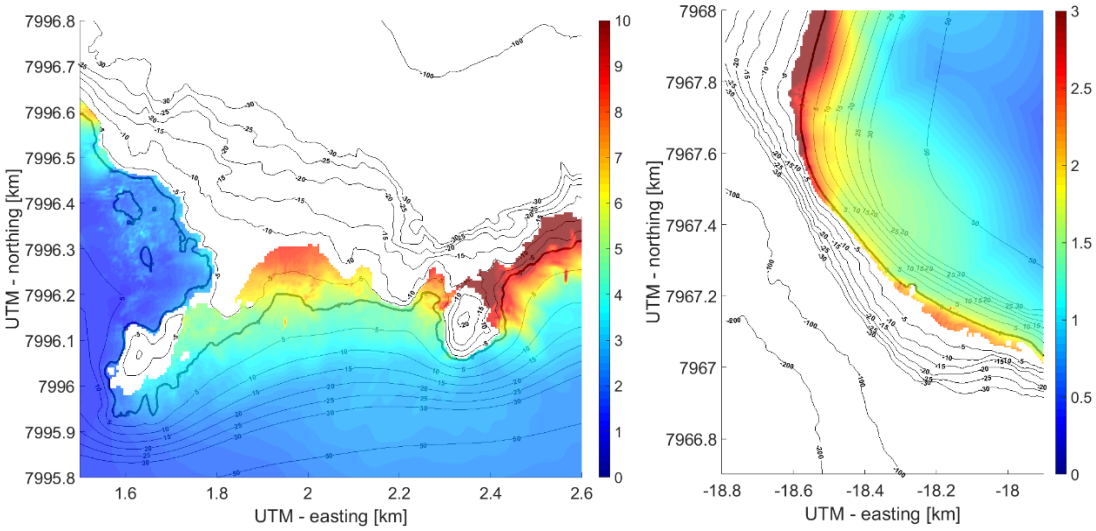

Figure B4-1: Maximum inundation heights (onshore values) and maximum water elevations (offshore values) for Nuugaatsiaq (left) and Illorsuit (right) for the 38Mm^3 10° friction angle Karrat 2017 simulation.

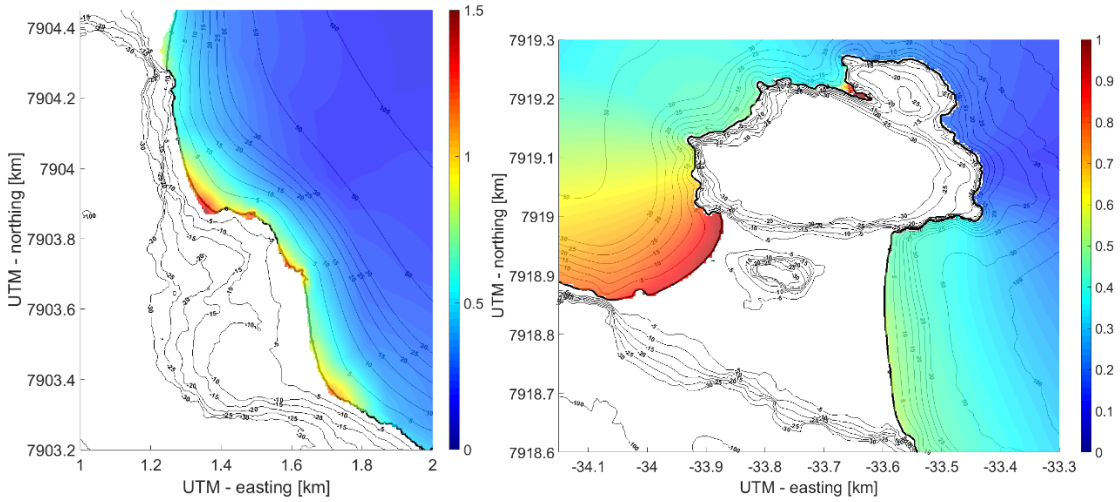

Figure B4-2: Maximum inundation heights (onshore values) and maximum water elevations (offshore values) for Qaarsut (left) and Niaqornat (right) for the 38Mm^3 10 °friction angle Karrat 2017 simulation.

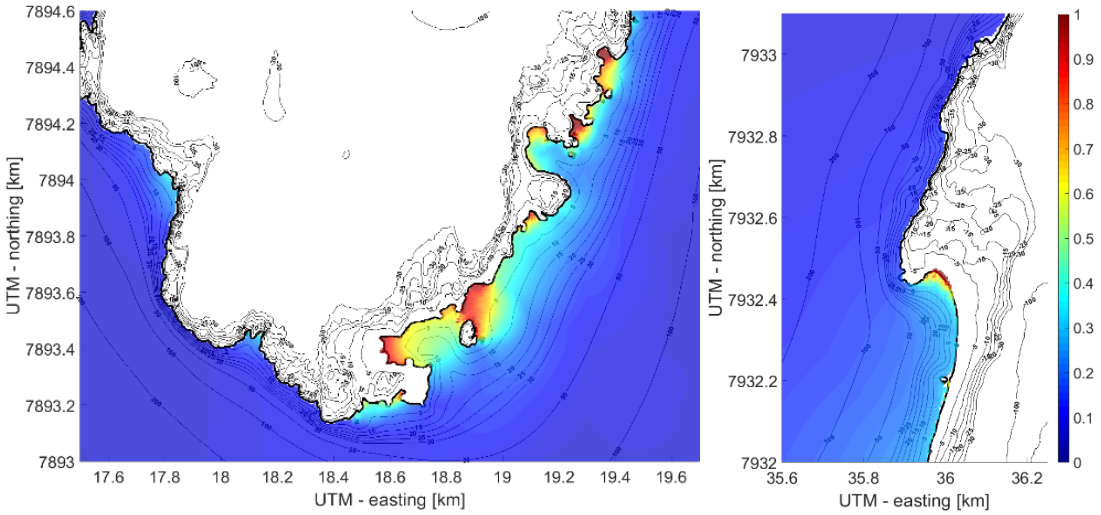

Figure B4-3: Maximum inundation heights (onshore values) and maximum water elevations (offshore values) for Uummannaq (left) and Ukkusissat (right) for the 38Mm^3 10 °friction angle Karrat 2017 simulation.

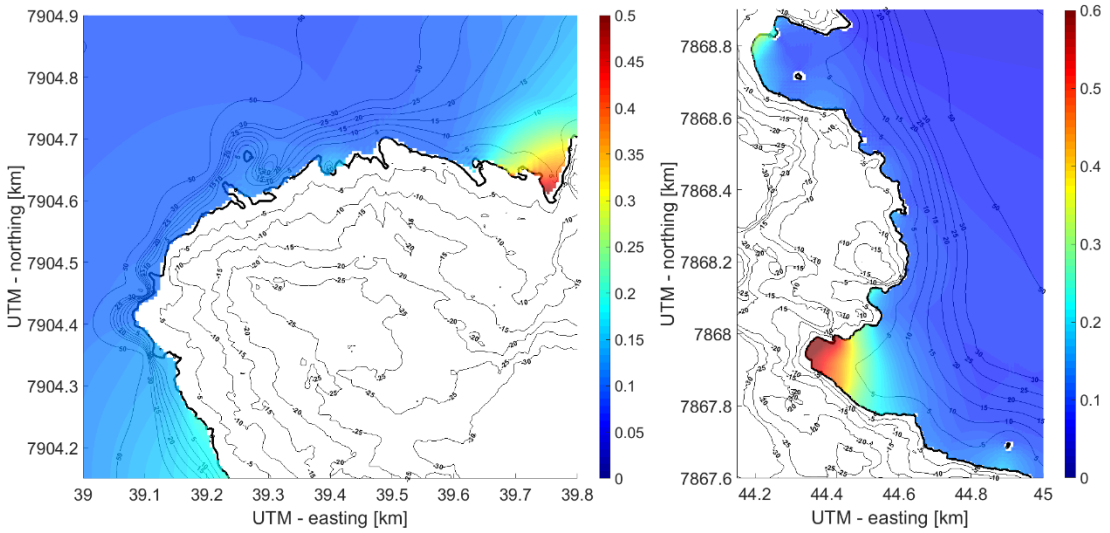

Figure B4-4: Maximum inundation heights (onshore values) and maximum water elevations (offshore values) for Saattut (left) and Ikerasak (right) for the 38Mm^3 10° friction angle Karrat 2017 simulation.

Appendix C

RESULTS FROM SCENARIO ANALYSIS

Contents

C1 Overview from modelling and assumptions

The landslide, tsunami generation, tsunami propagation, and inundation simulations were carried out using the four-step methodology outlined in Appendix A. The initial landslide shapes for the four scenarios Karrat 3 full, Karrat 3 lower, Karrat 1 and Karrat 2 (see the main body of the report) used in the models are shown in Figure C1-1. The landslide shapes were constructed based on the unstable slope areas shown in Figure C1-2, in close collaboration with GEUS. The initial landslide volumes for the scenarios were set up with a constant thickness over the unstable slope area. Volumes and thicknesses are listed in Table C1-1.

Table C1-1: Landslide scenario volumes and thicknesses.

Scenario	Slide Volume	Initial landslide thickness
Karrat 3 full	524 Mm^3	140.9 m
Karrat 3 lower	412 Mm^3	150.4 m
Karrat 1	13 Mm^3	42.3 m
Karrat 2	11 Mm^3	52.1 m

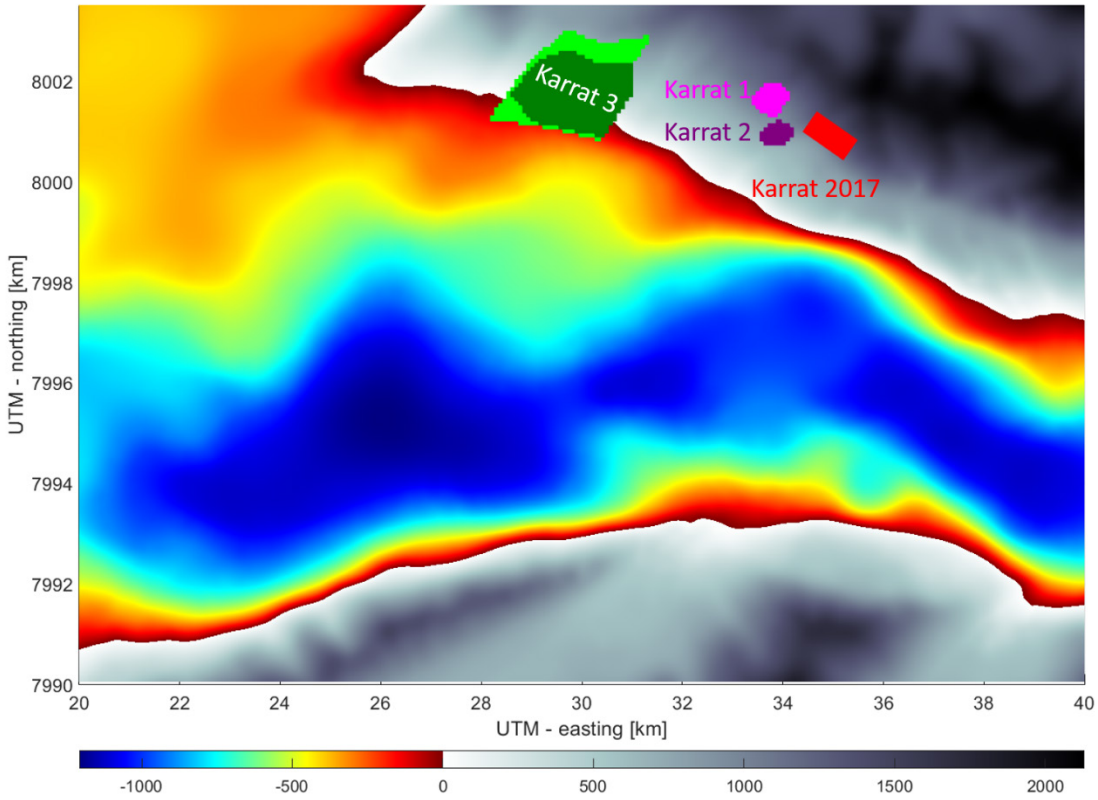

Figure C1-1: Location and extent of the different landslide volumes used for the scenario analysis. The outline of the initial 2017 landslide volume used for hindcasting (Appendix B) is also shown. The colour scale shows the water depth in meters.

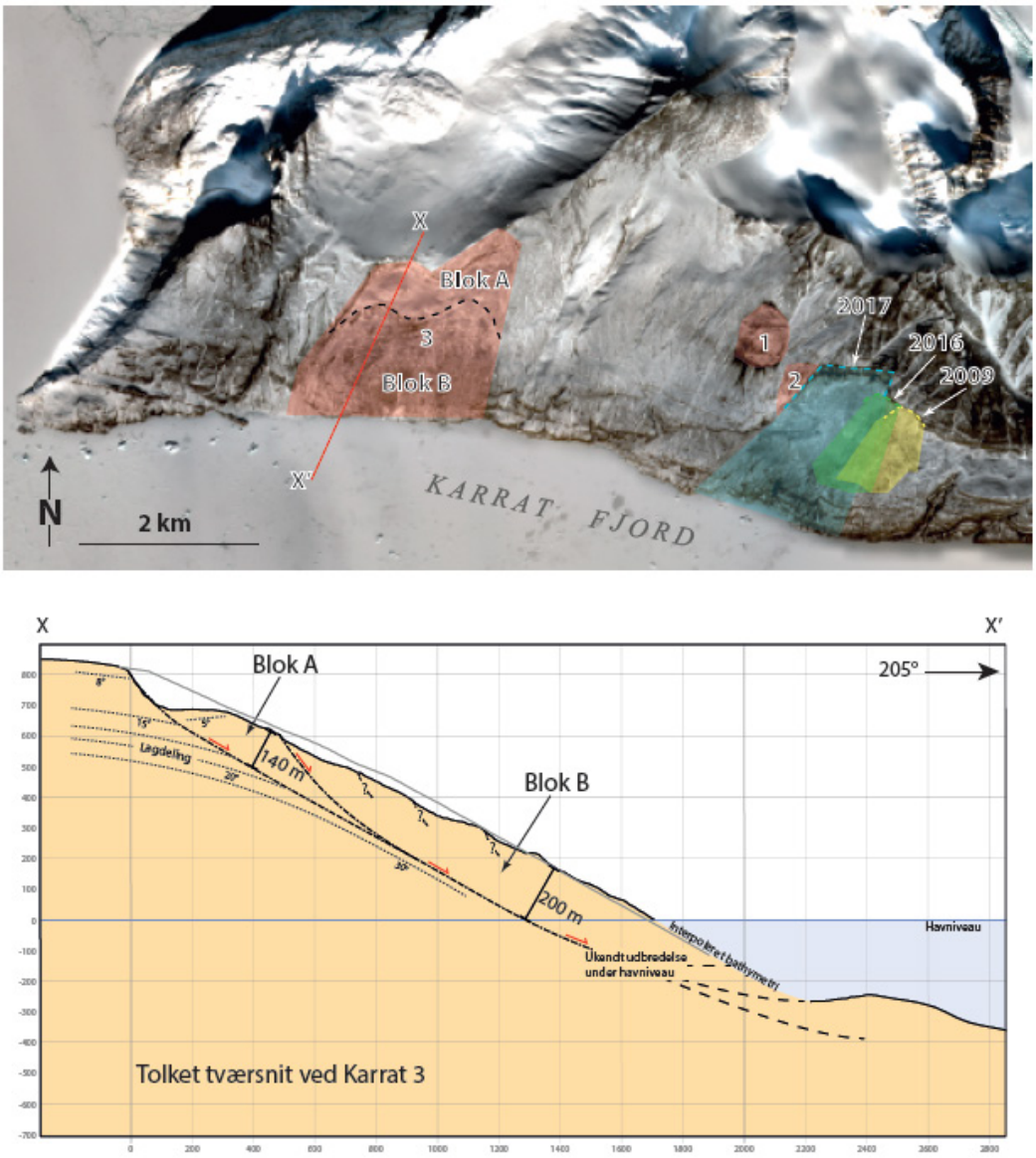

Figure C1-2: Landslide scenarios identified by Svennevig et al., (2019) (upper panel), and transect showing roughly estimated landslide thicknesses and vertical extents used as a basis for setting up the Karrat 3 scenarios (lower panel).

The 2017 event simulations and comparison with observed run-up heights presented in Appendix B are used as the basis for selecting the landslide parameters. As shown in Appendix B, the landslide simulations with friction angles of 5° and 10° provided the closest match with the run-up heights for the 2017 event, while the 15° provided a slight but distinct underestimation for Nuugaatsiaq where the most reliable and elaborate inundation data are found. On the other hand, the 15° friction angle simulation provided results that were compatible with far field tsunami wave observations. Hence, the Karrat 3 simulations were carried out for all of these model friction angles of 5°, 10°, and 15°, where the smallest friction angle represents the high (most conservative) estimate of the

tsunami, the 10 ° friction angle simulations the intermediate estimate, while the 15° friction angle simulations represent a low estimate. For the Karrat 1 and Karrat 2 scenarios, only the lowest friction angle of 5° was used, as these scenarios anyhow produced modest run-up heights for most of the locations.

The landslide simulations were carried out using a grid resolution of 20 m for total landslide duration of 240 s (Karrat 3), and 160 s (Karrat 1 and 2), providing landslide thickness as input to the tsunami simulations every 2 s. The corresponding tsunami simulations were carried out on a horizontal grid resolution of 100 m for a total duration of 2 hours. Grid refinement tests were undertaken to check model convergence. The local inundation simulations where run for a period of 1 hour after the first wave arrival, except for the two distal locations of Ukkusissat and Ikerasak, where the wave build-up took longer time, and the inundation simulations were carried out up to 1.5 hours after the first wave had arrived.

For most of the study locations, the same Manning friction parameter of $n = 0.03$ as for the 2017 event simulations were used. However, for Nuugaatsiaq and Karrat3 simulations very high waves and large inundated areas were found, and a higher friction angle of $n = 0.04$ was used for enhanced model stability only for this location. The larger friction will reduce the inundation slightly compared to the other sites, but this is not expected to influence the conclusions significantly. Similarly, different dry land threshold and minimum depth values were used for enhanced model stability purposes depending on the wave characteristics of the given study site, with the different values 1.0 m (Nuugaatsiaq), 0.5 m (Illorsuit), 0.3 m (Qaarsut, Niaqornat, Saattut, Ukkusissat), and 0.1 m (Uummannaq, and Ikerasak) used. The choice of these small numerical parameters does not influence the calculation of the final inundation distance significantly. Some of the topo-bathymetric data (Uummannaq, and Ukkusissat) were smoothed by a maximum gradient filter in ComMIT to mitigate model induced numerical noise and instabilities.

C2 Landslide run-out

Simulated final run-out distances for the Karrat 3 scenarios depend strongly on the friction angle used in the simulations. Final run-out distances for the full Karrat 3 scenario are shown for three different friction angles in Figure C2-1. Simulation with the 5° friction angle yields a final run-out distance entirely covering the deep part of the basin, while the 10° reaches the lower basin without spreading entirely across it. Most of the landslide mass for the 15° friction angle simulation stop on the shelf above the deepest part of the fjord, with only a smaller part reaching the deep fjord basin.

The simulated landslide run-out distances are compared with run-out distances observed previous landslide data (data provided by GEUS) through the *H/L* relationship, where *H* measures the total vertical drop height of the landslide and *L* the total horizontal run-out distance. This comparison is shown in Figure C2-2 for both Karrat 3 scenarios, and the 2017 landslide simulations. The groups of *H/L* relationships for the model simulations

are marked with dashed circles. The comparison shows that all the simulations for the 2017 event and the Karrat 3 simulations with friction angles of 5° and 10° seems to align along a similar trend line, while the Karrat 3 simulations with a friction angle of 15° deviate from this trend with higher *H/L* ratios. The 15° simulations also deviate slightly from main *H/L* trends in the empirical data, giving higher *H/L* ratios, although it must be noted that the data have significant uncertainty too. It is stressed that in this comparison, the *H/L* ratio for the 15° simulation uses the location of the main body of the final run-out, and neglects the small mass fraction that has entered into deep water. The short *H/L* ratio for this event may suggest that the 15° friction angle is in the higher end. Held together with the 2017 event simulation with a 15° friction angle that underpredicts the tsunami slightly in some places, this may suggest that this friction angle can be used as a parameter value that provides low estimates for the tsunami inundation. On the other hand, the 5° and 10° friction angles simulations provide long run-out distances, and for 5° the bathymetry acts as a barrier for the landslide preventing it from moving further. For these low values, the tsunami generation is also less sensitive to the friction angle. The 5° simulations provide a high estimate for the tsunami simulations.

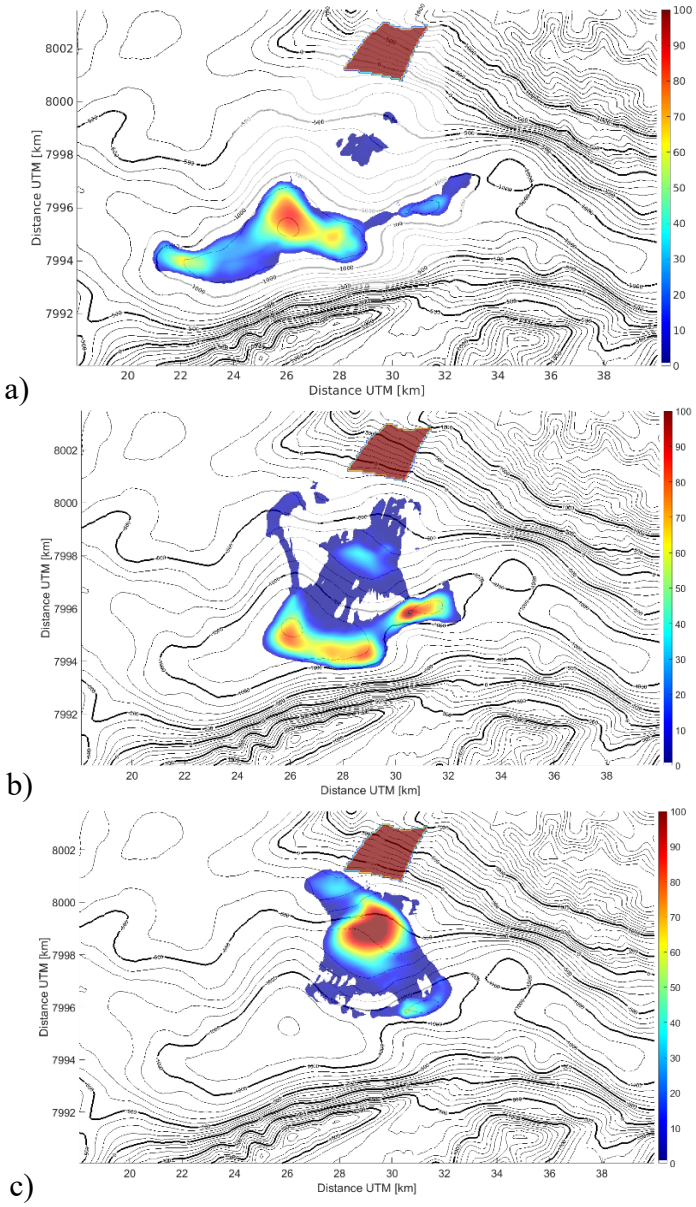

Figure C2-1: Example of simulated final run-out distances, Karrat 3 524 Mm³ slide volume. a) 5 ° friction angle, b) 10 ° friction angle, c) 15 ° friction angle.

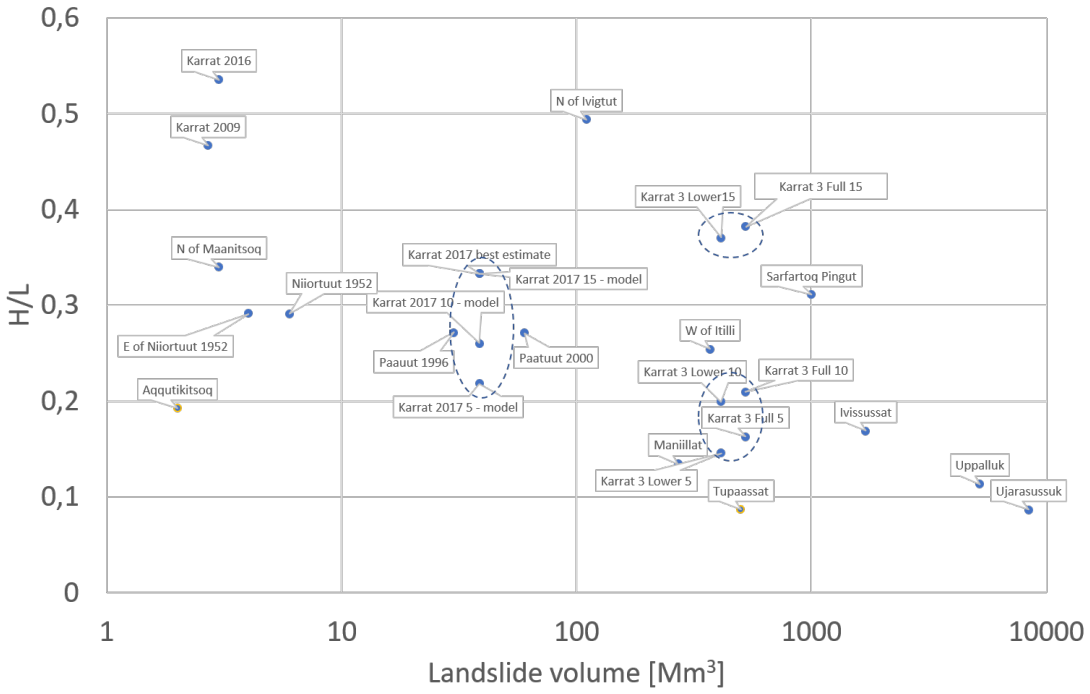

Figure C2-2: H/L curve for past landslides in Greenland plotted together with simulated H/L for the 38.5 Mm³ Karrat 2017 simulations and the Karrat 3 scenarios for friction angles 5°, 10°, and 15°. The blue dashed circles highlight the H/L ratios and volumes for the model simulations conducted here.

C3 Simulated run-up heights

An overview of the simulated run-up heights from the tsunami inundation simulations for the Karrat 3 full volume scenario grouped by the applied friction angles and study locations are shown in Table C3-1, while the corresponding overview of the lower part of Karrat 3 is shown in Table C3-2. Simulated run-up heights for and maximum water levels for the much smaller Karrat 1 and Karrat 2 are given Table C3-3. Discussions of the main findings related to the run-up heights from these simulations are found in the main body of this report. Below, we provide a short discussion related to uncertainty of the simulations, which supplements the discussion given in the main body of the report. The discussion include a set of figures (Figure C3-1, Figure C3-3, Figure C3-5, and Figure C3-7) that show the maximum inundation extents, and examples of maximum inundation heights (Figure C3-2, Figure C3-4, Figure C3-6, and Figure C3-8). The maximum inundation limits in Figure C3-1, Figure C3-3, Figure C3-5, and Figure C3-7 include the following information:

i) High estimate (friction angle of 5°) maximum horizontal inundation limit for the full and lower Karrat 3 landslide volume simulations relative to the mean sea level without added tide.

ii) Low estimate (friction angle of 15°) maximum horizontal inundation limit from the full and lower Karrat 3 landslide volume simulations relative to the mean sea level without added tide.
iii) Maximum horizontal inundation limit due to both Karrat 3 landslide volume simulations where a 2 m spring tide is drawn manually on top of the high estimate simulations. Adding this additional tidal elevation was done in agreement with GEUS.
iv) Maximum horizontal inundation limit for Karrat 1 and Karrat 2 landslide volume simulations with a 2 m spring tide drawn manually (only shown for Nuugaatsiaq and Illorsuit in Figure C3-1).

*Table C3-1: Maximum run-up heights due to the Karrat 3 scenario representing the full part of the slope with a volume of 524 Mm^3 for the three friction angles 5°, 10°, and 15°. All values refer to mean sea level without added tide. *Localized run-up heights in one single bay area, lower values elsewhere. **Wave overran a small part of the left boundary of the computational domain.*

Location	High estimate - 5°	Mid estimate - 10°	Low estimate - 15°
Nuugaatsiaq	35 – 72 m	24 - 62 m	19 – 54 m
Illorsuit**	18 – 41 m	18 - 36 m	11 – 25 m
Qaarsut	9 - 21 m	7 - 18 m	4 – 11 m
Niaqornat	9 - 15 m	7 - 13 m	4 – 8 m
Uummannaq	4 – 12 m	4 – 10 m	3 – 8 m
Saattut	3 – 8.5 m*	2 - 8 m*	1.5 – 5 m
Ukkusissat	3.5 – 5.5 m	3.5 – 5.5 m	2.0 – 3.5 m
Ikerasak	2.5 – 9 m*	2 – 7 m*	1.5 – 5 m

*Table C3-2: Maximum run-up heights due to the Karrat 3 scenario representing the unstable lower part of the slope with a volume of 412 Mm^3 for the three friction angles 5°, 10°, and 15°. All values refer to mean sea level without added tide. *Localized run-up heights in one single bay area, lower values elsewhere. **Wave overran a small part of the left boundary of the computational domain.*

Location	Highest estimate - 5°	Mid estimate - 10°	Low estimate - 15°
Nuugaatsiaq	30 – 70 m	27 - 63 m	16 – 50 m
Illorsuit	17 – 33 m	15 – 30 m	12 – 25 m
Qaarsut	7 – 18 m	6 – 14 m	4 – 10 m
Niaqornat	7 - 12 m	6 – 12 m	4 – 7.5 m
Uummannaq	4 – 11 m	4 – 8 m	3 – 7 m
Saattut	2 – 8.5 m*	1.5 – 8 m*	1.2 – 4.5 m
Ukkusissat	3 – 4.5 m	3 – 4 m	2.0 – 3.5 m
Ikerasak	2 – 8 m*	2 – 7 m*	1.5 – 4.5 m

*Table C3-3: Maximum water levels and run-up heights for the Karrat 1 and Karrat 2 scenarios. All values refer to mean sea levels without added tide. *Values refer to offshore water level, the wave did not inundate significantly.*

Location	Karrat 1	Karrat 2
Nuugaatsiaq	4 m	4 m
Illorsuit	1.7 m	1.9 m
Qaarsut*	0.5 m	0.5 m
Niaqornat*	0.25 m	0.3 m
Uummannaq*	0.6 m	0.6 m
Saattut*	0.15 m	0.17 m
Ukkusissat*	0.2 m	0.15 m
Ikerasak*	0.2 m	0.2 m

Figure C3-1 shows the maximum inundation limits for simulations for the Nuugaatsiaq and Illorsuit locations. Figure C3-2 shows the maximum inundation heights for the 524 Mm^3 10° friction angle scenario for the same two locations. Simulations for Nuugaatsiaq and Illorsuit give extreme run-up heights, with tsunami run-up heights invariably above 20 m, in some areas even exceeding 70 m. Horizontal inundation distances can range beyond 500 m inland (Nuugaatsiaq). While clearly lower run-up heights are found in the lower bound estimates, even these simulations predict complete inundation of both sites.

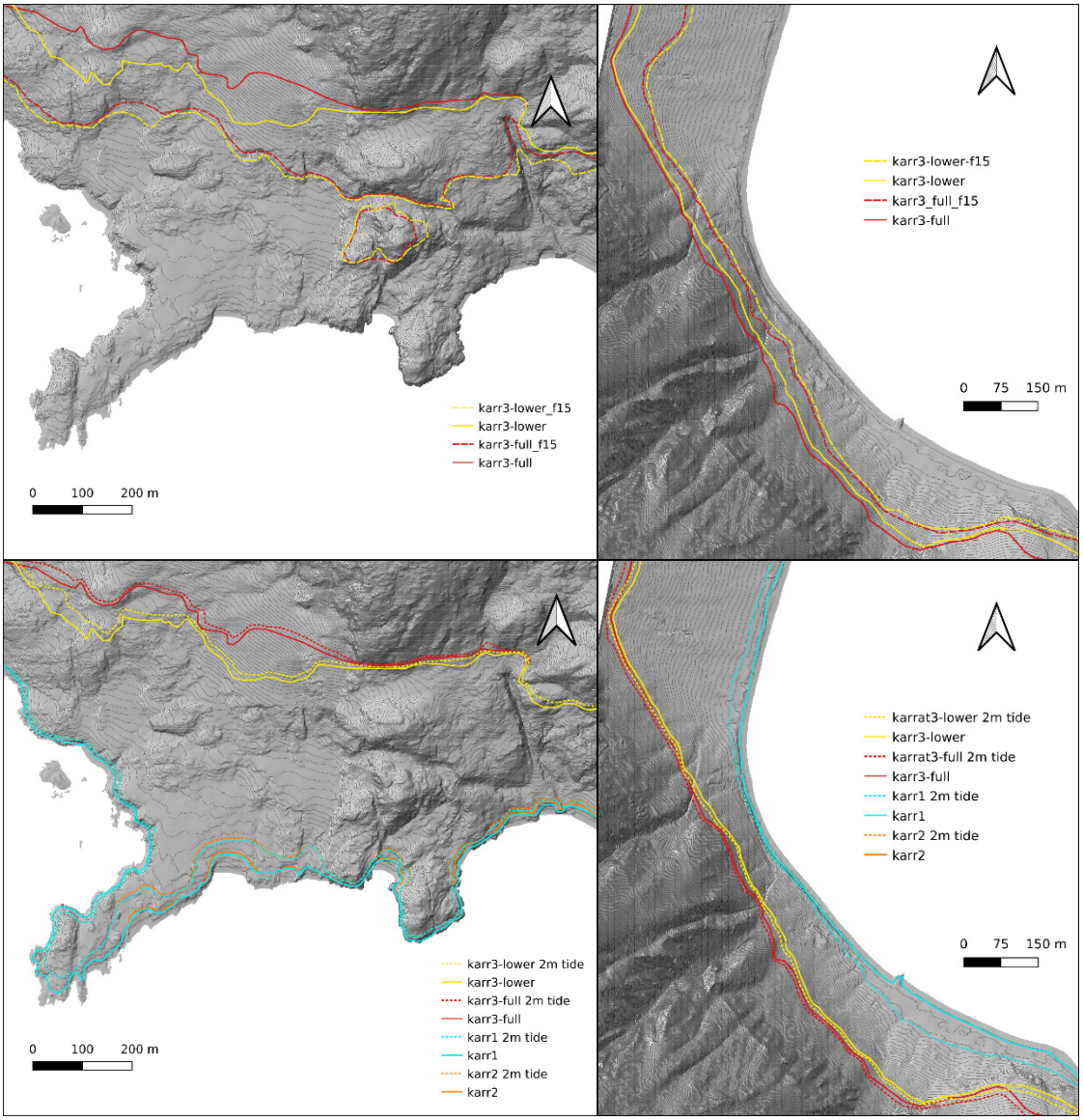

Figure C3-1: Modelled maximum tsunami inundation limits for different scenarios for Nuugaatsiaq (left) and Illorsuit (right). Upper panel, high and low (labelled "f15") estimates for the full and lower Karrat 3 scenarios. Lower panel, high estimates with and without added tide for all scenarios. Red curves refer to Karrat 3 (524 Mm^3), yellow lines to Karrat 3 (412 Mm^3), brown lines to Karrat 2, turquoise lines to Karrat 1.

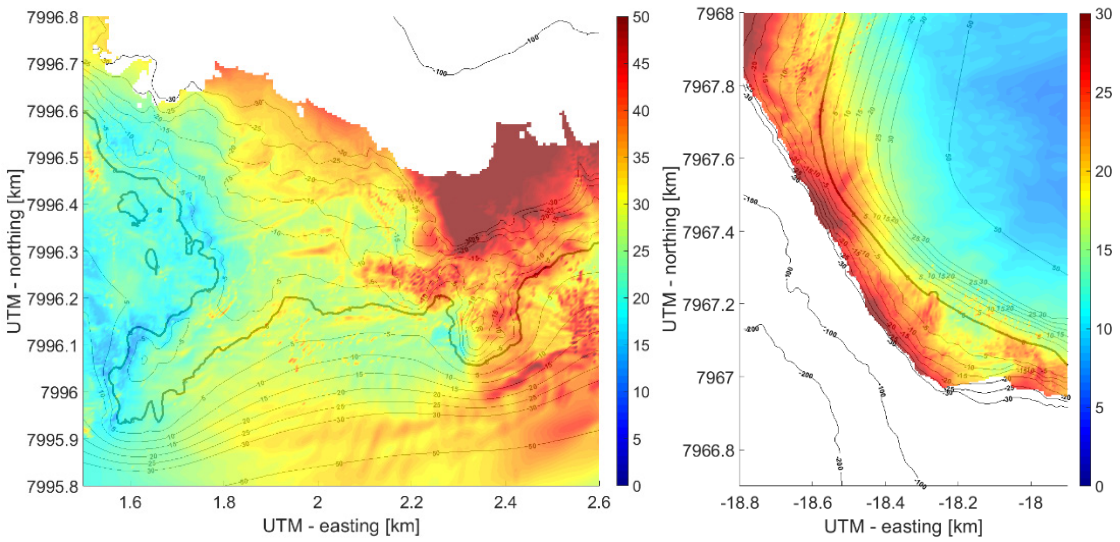

Figure C3-2: Maximum inundation heights (onshore values) and maximum water elevations (offshore values) for Nuugaatsiaq (left) and Illorsuit (right) for the 512 Mm³ 10° friction angle Karrat 3 full simulation.

Figure C3-3 shows the maximum inundation limits for simulations for the Qaarsut and Niaqornat locations. Figure C3-4 shows the maximum inundation heights for the 524 Mm^3 10° friction angle scenario for the same two locations. For the Qaarsut village the high estimate modelling predicts up to 21 m run-up height (without added tide), with horizontal inundation distances in the south part of the village up to about 300 m. This is obtained for the most conservative scenario (524 Mm^3, 5° friction angle, with 2 m spring tide). However, there is a significant uncertainty related to the simulations. With the smaller volume and higher friction angles, the run-up heights are still high but significantly smaller than for the high estimates, with horizontal inundation extents reaching less than half the distance than for the high estimate. Adding 2 m tide also influences the horizontal extent significantly. The simulated maximum run-up height for the village of Niaqornat are smaller than for Qaarsut, up to 15 m high, but because the settlement area is low lying all scenarios predict complete inundation of the settlement area. The extent of the inundation is therefore less sensitive to the landslide generation and the tide here than for Qaarsut, as the steep topography largely controls the inundation, and because all the buildings are located below the trim line and would be completely inundated.

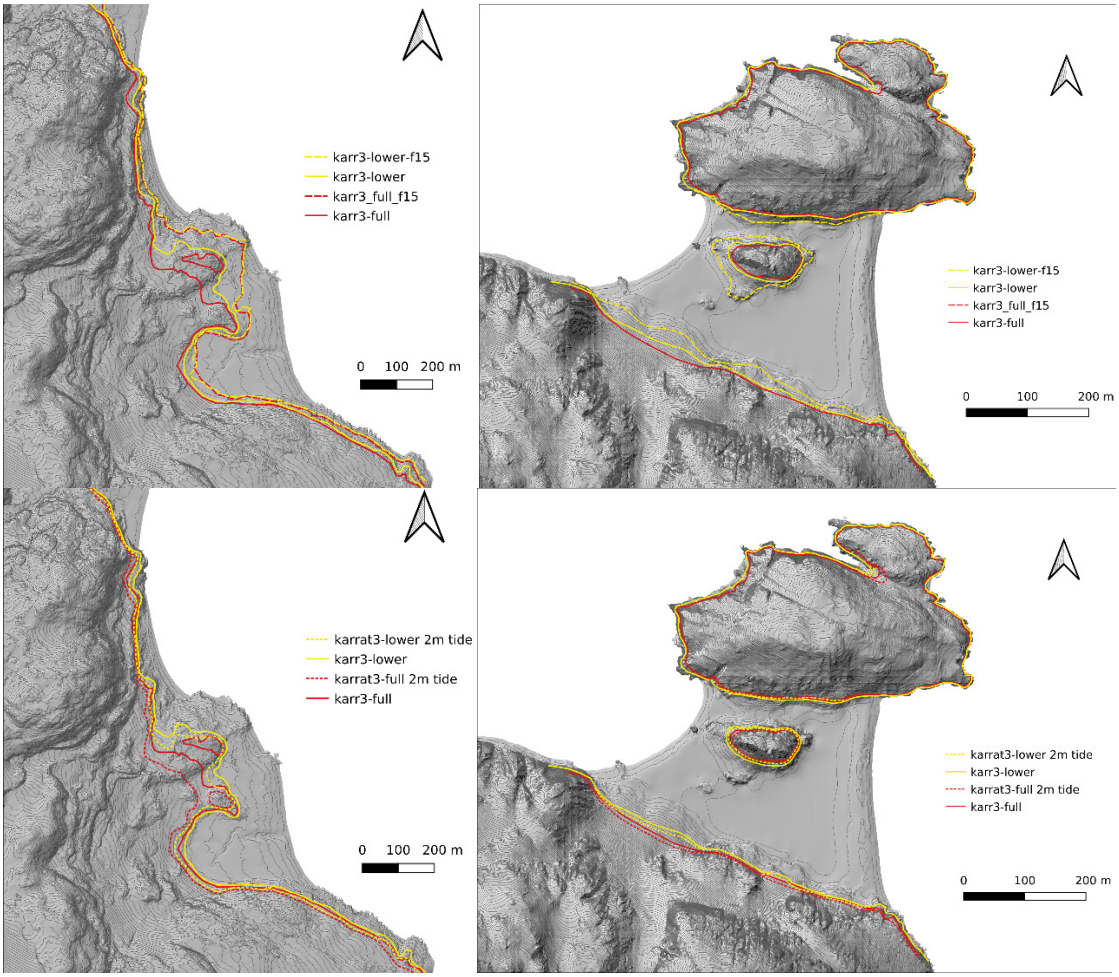

Figure C3-3: Modelled maximum tsunami inundation limits for different scenarios for Qaarsut (left) and Niaqornat (right). Upper panel, high and low (labelled "f15") estimates for the full and lower Karrat 3 volume scenarios. Lower panel, high estimates (friction angle of 5°) with and without added tide for both Karrat 3 volume scenarios. Red curves refer to Karrat 3 (524 Mm^3), yellow lines to Karrat 3 (412 Mm^3).

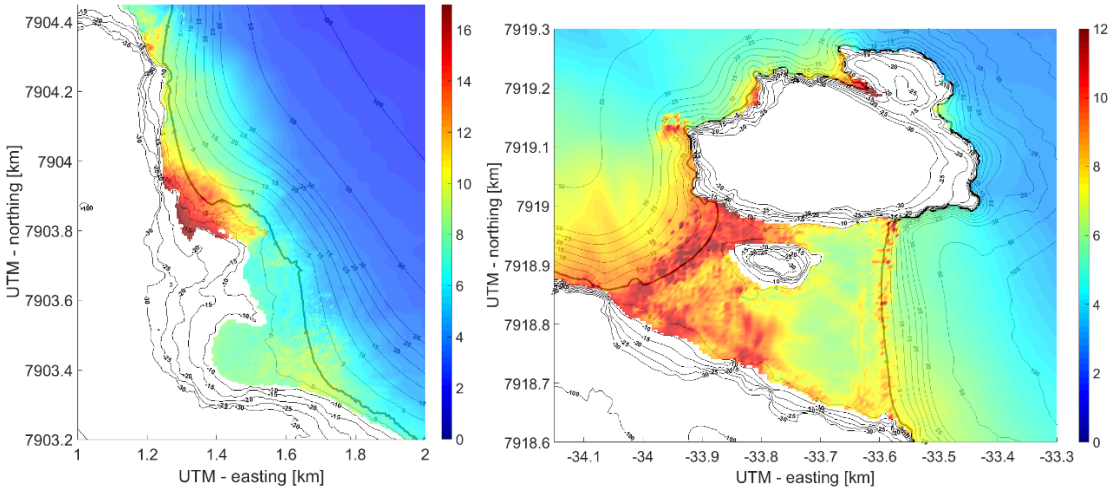

Figure C3-4: Maximum inundation heights (onshore values) and maximum water elevations (offshore values) for Qaarsut (left) and Niaqornat (right) for the 512 Mm³ 10° friction angle Karrat 3 full simulation.

Figure C3-5 shows the maximum inundation limits for simulations for the Uummannaq and Ukkusissat locations. Figure C3-6 shows the maximum inundation heights for the 524 Mm^3 10° friction angle scenario for the same two locations. High estimate model simulations for Uummannaq predict high waves for part of the inhabited area, up to 12 m (full Karrat 3 volume) run-up height and over more than 100 m horizontal inundation in the southernmost bay area where critical infrastructure is located. There is a significant uncertainty related to the simulations, with lower bound estimates giving a maximum of 8 m maximum run-up height for the 15° friction angle scenario. However, the larger populated part of the Uummannaq is located outside the inundated zone. The village of Ukkusissat faces inundation up to 5.5 m, limited to the bay area. The maximum horizontal inundation limit is 50-75 m. While the run-up heights and the inundated area is smaller than for all other study sites, the inundation limits encompass several buildings. However, the uncertainty is appreciable, and the lower estimates give more run-up heights up to 3.5 m and a clearly smaller inundated area.

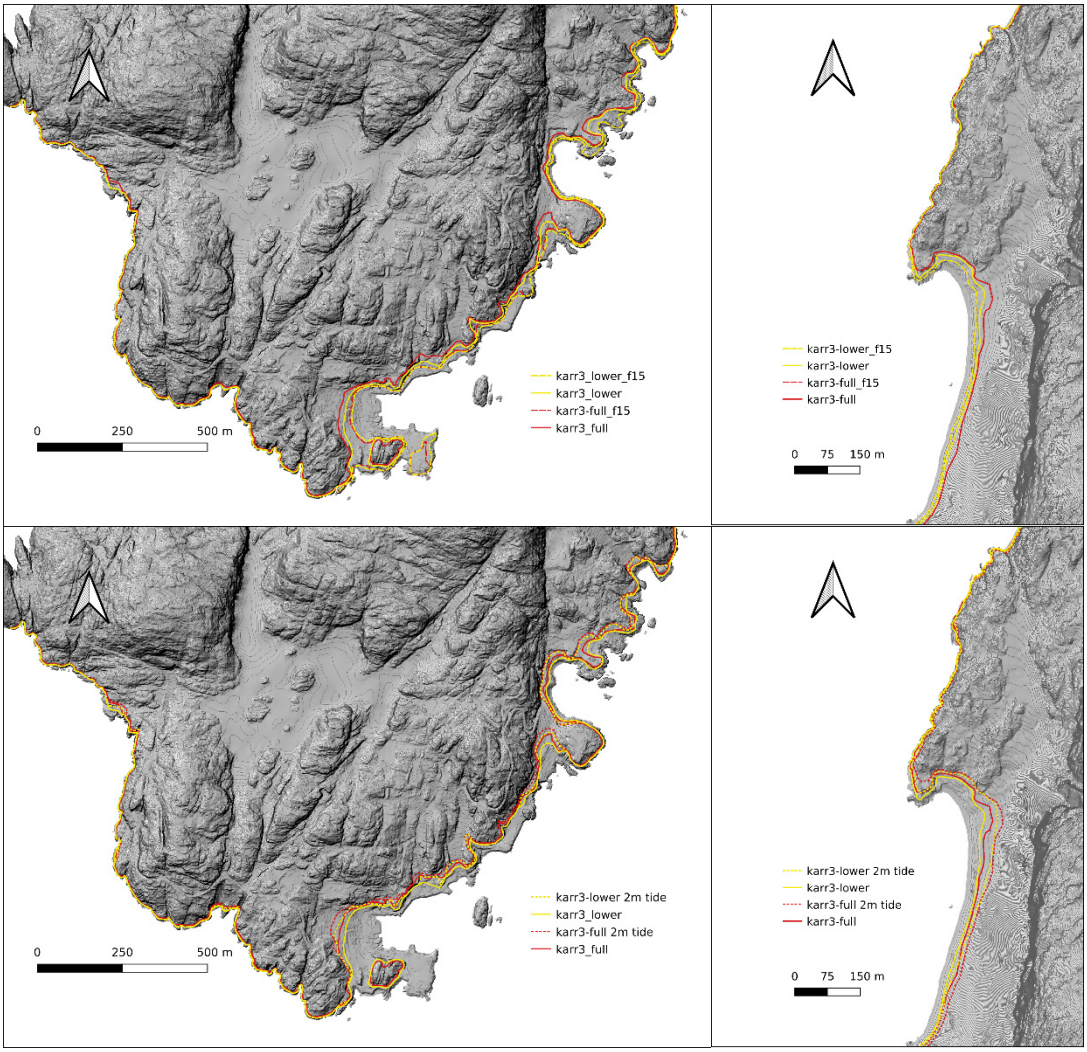

Figure C3-5: Modelled maximum tsunami inundation limits for different scenarios for Uummannaq (left) and Ukkusissat (right). Upper panel, high and low (labelled "f15") estimates for the full and lower Karrat 3 scenarios. Lower panel, high estimates with and without added tide for all scenarios. Red curves refer to Karrat 3 (524 Mm^3), yellow lines to Karrat 3 (412 Mm^3).

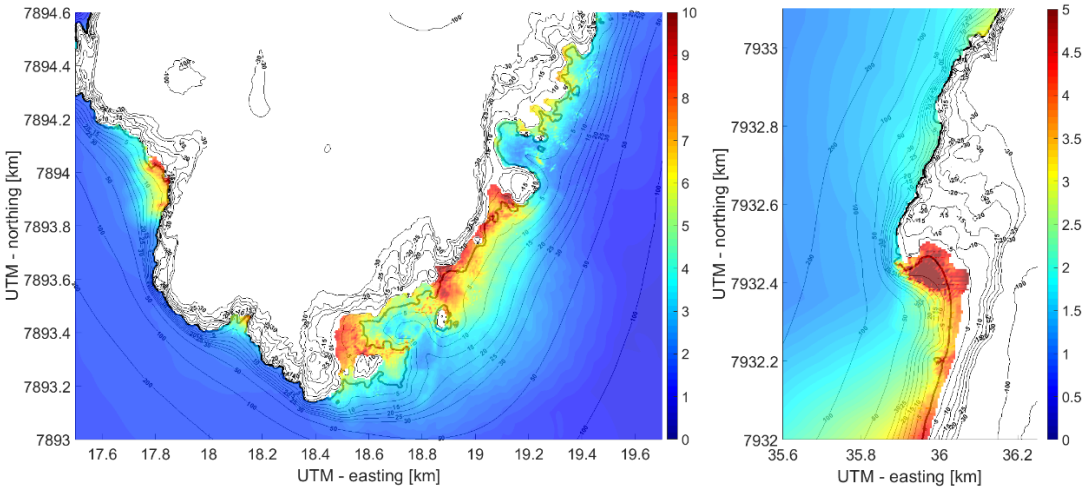

Figure C3-6: Maximum inundation heights (onshore values) and maximum water elevations (offshore values) for Uummannaq (left) and Ukkusissat (right) for the 512 Mm^3 10° friction angle Karrat 3 full simulation.

Figure C3-7 shows the maximum inundation limits for simulations for the Saattut and Ikerasak locations. Figure C3-8 shows the maximum inundation heights for the 524 Mm^3 10° friction angle scenario for the same two locations. Model simulations predict that the village of Saattut faces limited inundation, with the exception of a run-up height of 7-8.5 m with a horizontal inundation of about 100 m confined to the northern bay area for the high estimate simulations (both volumes). For the lower bound estimates, there is relatively limited inundation. The shape of the bay amplifies the inundation due to focussing. Model simulations for the village of Ikerasak show maximum run-up heights up to 7-9 m, but these large heights are restricted to one single bay area, as the high waves are caused by the local conditions of the bay amplifying the waves. For the remaining we find moderate run-up heights of 1.5-4 m. As for Saattut, there is a large uncertainty as the lower bound estimate gives moderate horizontal inundation. As shown in Figure C3-7, the presence of high tide can increase the inundation extents significantly in some low-lying areas.

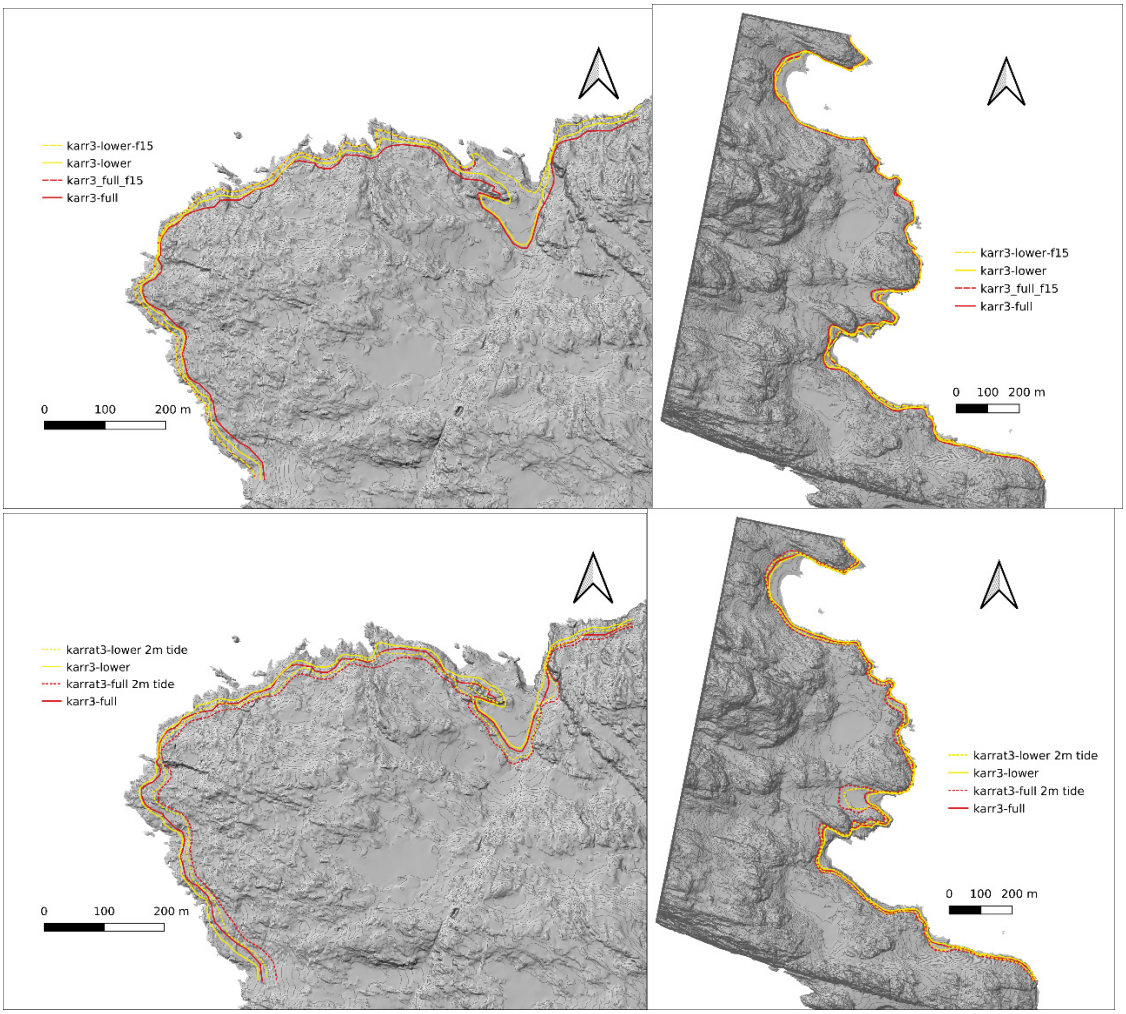

Figure C3-7: Modelled maximum tsunami inundation limits for different scenarios for Saattut (left) and Ikerasak (right). Upper panel, high and low (labelled "f15") estimates for the full and lower Karrat 3 scenarios. Lower panel, high estimates with and without added tide for all scenarios. Red curves refer to Karrat 3 (524 Mm^3), yellow lines to Karrat 3 (412 Mm^3).

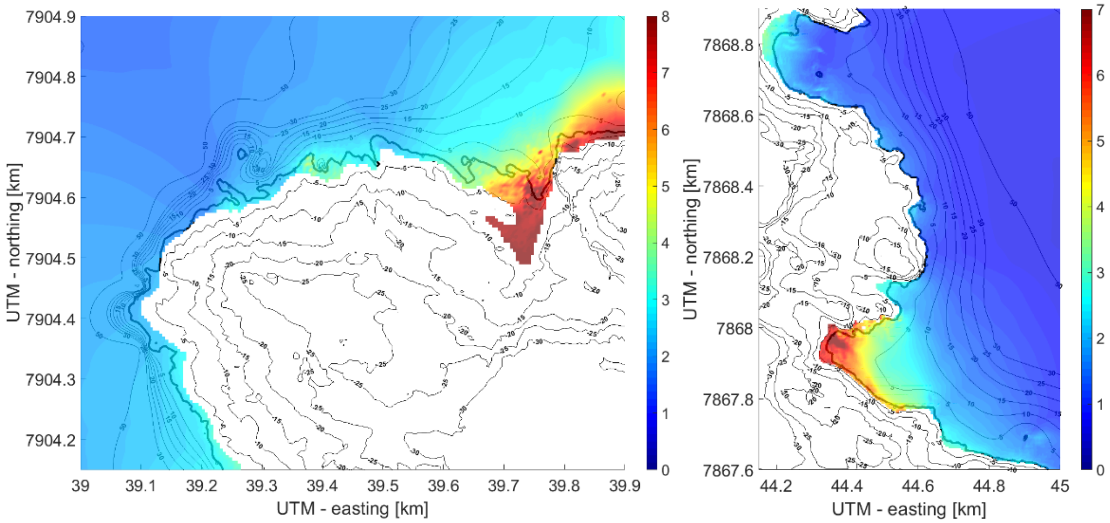

Figure C3-8: Maximum inundation heights (onshore values) and maximum water levels (offshore values) for Saattut (left) and Ikerasak (right) for the 512Mm³ 10 ° friction angle Karrat 3 full simulation.

Kontroll- og referanseside/ Review and reference page

Dokumentinformasjon/*Document information*		
Dokumenttittel/*Document title* Tsunami hazard screening for the Uummannaq fjord system - Greenland		**Dokumentnr./*Document no.*** 20200823-01-R
Dokumenttype/*Type of document* Rapport / Report	**Oppdragsgiver/*Client*** GEUS	**Dato/*Date*** 2021-03-26
Rettigheter til dokumentet iht kontrakt/ *Proprietary rights to the document according to contract* NGI		**Rev.nr.&dato/*Rev.no.&date*** 0 /
Distribusjon/*Distribution* BEGRENSET: Distribueres til oppdragsgiver og er tilgjengelig for NGIs ansatte / LIMITED: Distributed to client and available for NGI employees		
Emneord/*Keywords* Tsunamis, rock slides, Karratfjorden, Greenland		

Stedfesting/*Geographical information*	
Land, fylke/*Country* Denmark, Greenland	**Havområde/*Offshore area*** Karratfjorden
Kommune/*Municipality*	**Feltnavn/*Field name***
Sted/*Location*	**Sted/*Location***
Kartblad/*Map*	**Felt, blokknr./*Field, Block No.***
UTM-koordinater/*UTM-coordinates* **Zone: East: North:**	**Koordinater/*Coordinates*** **Projection, datum: East: North:** **71°38'24.7"N 52°30'43.8"W**

Dokumentkontroll/*Document control*

Kvalitetssikring i henhold til/*Quality assurance according to NS-EN ISO9001*

Rev/ *Rev.*	**Revisjonsgrunnlag/*Reason for revision***	**Egenkontroll av/ *Self review by:***	**Sidemanns-kontroll av/ *Colleague review by:***	**Uavhengig kontroll av/ *Independent review by*:**	**Tverrfaglig kontroll av/ *Interdisciplinary review by:***
0	Oirignal document	2021-03-26 Finn Løvholt	2021-03-26 Sylfest Glimsdal	2021-03-26 Carl B Harbitz	

Dokument godkjent for utsendelse/ *Document approved for release*	**Dato/*Date***	**Prosjektleder/*Project Manager***
	26 March 2021	Finn Løvholt

NGI (Norwegian Geotechnical Institute) is a leading international centre for research and consulting within the geosciences. NGI develops optimum solutions for society and offers expertise on the behaviour of soil, rock and snow and their interaction with the natural and built environment.

NGI works within the following sectors: Offshore energy – Building, Construction and Transportation – Natural Hazards – Environmental Engineering.

NGI is a private foundation with office and laboratories in Oslo, a branch office in Trondheim and daughter companies in Houston, Texas, USA and in Perth, Western Australia

www.ngi.no

NGI (Norges Geotekniske Institutt) er et internasjonalt ledende senter for forskning og rådgivning innen ingeniørrelaterte geofag. Vi tilbyr ekspertise om jord, berg og snø og deres påvirkning på miljøet, konstruksjoner og anlegg, og hvordan jord og berg kan benyttes som byggegrunn og byggemateriale.

Vi arbeider i følgende markeder: Offshore energi – Bygg, anlegg og samferdsel – Naturfare – Miljøteknologi.

NGI er en privat næringsdrivende stiftelse med kontor og laboratorier i Oslo, avdelingskontor i Trondheim og datterselskaper i Houston, Texas, USA og i Perth, Western Australia.

www.ngi.no

NGI
OSLO
TRONDHEIM
HOUSTON
PERTH

NORWEGIAN GEOTECHNICAL INSTITUTE
NGI.NO

Main office
PO Box 3930 Ullevaal St.
NO-0806 Oslo
Norway

Trondheim office
PO Box 5687 Torgarden
NO-7485 Trondheim
Norway

T (+47)22 02 30 00
F (+47)22 23 04 48
NGI@ngi.no

BIC NO. DNBANOKK
IBAN NO26 5096 0501 281
ORGANISATION NO.
958 254 318MVA

ISO 9001/14001
CERTIFIED BY BSI
FS 32989/EMS 612006